



CELL-INTEGRATED SENSING FUNCTIONALITIES FOR SMART BATTERY SYSTEMS
WITH IMPROVED PERFORMANCE AND SAFETY

GA 957273

D5.1 - TEST REPORT ON CELL AND MODULE PERFORMANCE
AND SAFETY

LC-BAT-13-2020 - Sensing functionalities for smart battery cell chemistries



Deliverable No.	5.1	
Related WP	5	
Deliverable Title	Test report on cell and module performance and safety	
Deliverable Date	22-12-2023	
Deliverable Type	REPORT	
Dissemination level	Public (PU)	
Written By	Bernd Eschelmüller (AIT)	11-10-2023
	Gregor Glanz (AIT)	16-10-2023
	Katja Fröhlich (AIT)	17-10-2023
	Harald Kren (VAR)	21-11-2023
	Unai Echeverria (IKE)	17-12-2023
	Glen Vandenbempt (FM)	19-12-2023
	Henk Jan Bergveld (TUE/NXP-NL)	20-12-2023
	Jasmin Smajic (ABEE)	21-12-2023
Checked by	Bernd Eschelmüller (AIT)	22-12-2023
Reviewed by	Iñigo Gandiaga (IKE)	22-12-2023
	Jasmin Smajic (ABEE)	21-12-2023
Approved by	Iñigo Gandiaga (IKE)	22-12-2023
Status	Final	22-12-2023



Summary

The report presents the activities carried out in the framework of task 5.1 "Validation testing of cells and testing of modules" and shows the results obtained in relation to the objectives of SENSIBAT.

The main objective was to test and validate the baseline and prototype cells with Level 1 and Level 2 sensors and the module in order to assess effects the sensors may have on functionality, performance, safety, ageing/degradation. The influence of the integration of the developed sensor units on the main performance indicators of the cells such as complex resistance, discharge capacity at certain C-rates and ohmic pulse discharge resistance of the cells was validated by performing various tests according to the document D1.2 [2]. Additional safety tests were carried out with all the different cell configurations to assess the impact of implementing sensors on safety.

In addition, the test data obtained during the cycle were used for the development of algorithms for advanced state estimation based on level 1 and level 2 sensor information. The validation of the added value of the integration of sensor units was carried out as well. No major influence of the sensor implementation on the electrochemical performance of the cells could be detected by performing following tests:

- Performance Test
- EIS
- Calendar life test
- Cycle life test
- Pulse-discharge test
- Drive-cycle test

Long-term cell storage has shown that the L1 sensor integration has a long-term influence on the integrity of individual cell components. It can be assumed that the used material combination for the L1 sensor encapsulation (Parylene C) and the melting layer of the pouch foil (PP) does not produce a satisfactory sealing.

This deliverable and the related task include deviations from the objectives planned in the Grant Agreement of the SENSIBAT project. The stated goal of "Validated final pouch cells with integrated (Level 1 and Level 2) sensors meeting the requirements specified in WP1" was only partially achieved. Unexpected influences such as higher production quality deviations and transport effects led to lower reproducibility and lower performance values of some of the tested prototype, L1 and L2 cells. Furthermore, difficulties in the development and production of the L1 sensors to be implemented as well as in the development and production of the readout circuit and the implementation process development of the sensor units led to less satisfactory results than expected. Due to the difficulties mentioned above, the defined goal of "Validated final modules including BMS that meet the requirements set out in WP1" was also only partially achieved.



Table of Contents

1	Introduction	8
2	Testing Plan.....	9
3	Data Storage for Result Analysis	10
4	Cell Testing and Validation.....	11
4.1	Performance Test	11
4.2	Calendar Life, Cycle Life, (long-term behaviour).....	15
4.3	EIS Results.....	20
4.4	Pulse DCH, Drive-cycle.....	22
4.5	Post-mortem Analysis	23
4.5.1	Risk Mitigation	28
4.6	Safety	30
4.6.1	Information on the performed Safety Tests	30
4.6.2	Safety Test 1: Nail penetration Test.....	32
4.6.3	Safety Test 2: Heating Test.....	34
4.6.4	Safety Test 2: Overcharge Test.....	37
5	Algorithm validation.....	39
6	Module and Component Validation.....	48
6.1	Functional Safety Analysis	50
7	Discussion & Conclusion	51
8	References	52
9	Acknowledgement	53



Table of Figures

Figure 1: Conducted Performance Test on a baseline 5 Ah pouch cell.....	11
Figure 2: Capacity over cycles comparison of BL-5Ah and L1-5Ah pouch cells. This corresponds to the “check-up” & “capacity and energy” part of the Performance Test.....	12
Figure 3: Power during charging of BL-5Ah and L1-5Ah pouch cells at three different SOC levels for three different C-rates. This corresponds to the “power and resistance” part of the Performance Test.....	13
Figure 4: Capacity over cycles comparison of BL-1Ah and L2-1Ah pouch cells. This corresponds to the “check-up” & “capacity and energy” part of the Performance Test part.....	14
Figure 5: Power during charging of BL-1Ah L2-1Ah pouch cells at three different SOC levels for three different C-rates. This corresponds to the “power and resistance” part of the Performance Test.....	14
Figure 6: Capacity evolution over cycles in three L1-5Ah pouch cells.....	16
Figure 7: Internal resistance evolution over cycles in three L1-5Ah pouch cells.....	16
Figure 8: Capacity and internal resistance evolution over cycles in three L1-5Ah pouch cells and two BL-5Ah cells.....	17
Figure 9: Details of the external pressure measurement setup for L1-5Ah cells.....	18
Figure 10: Capacity evolution over time in two L1-5Ah pouch cells and three BL-5Ah cells.....	19
Figure 11: Internal resistance evolution over time in two L1-5Ah pouch cells and three BL-5Ah cells.....	19
Figure 12: EIS plot of BL-5Ah pouch cell vs. L1-5Ah pouch cell.....	20
Figure 13: EIS plot of BL-1Ah pouch cell vs. L1-1Ah pouch cell vs. L2-1Ah pouch cell.....	21
Figure 14: Current (red, right-hand-side y axis), cell voltage (blue, voltage y-axis up to 4.25V) and reference potential (LFP versus graphite; black, voltage y-axis up to 3.35V) for a pulsed discharge test.....	22
Figure 15: Current (red), cell voltage (blue) and reference potential (LFP versus graphite; black) for a drive-cycle test.....	23
Figure 16: BL-5Ah pouch cell post-mortem components including cathode (left), anode (middle) and separator sheet (right).....	24
Figure 17: Visual assessment of the BL-1Ah anode (left) and cathode (right).....	24
Figure 18: Visual assessment of the L1-1Ah anode (left) and cathode (right).....	25
Figure 19: XPS of BL-1Ah and L1-1Ah anodes either from the middle or the edge of the electrodes stack.....	25
Figure 20: Visual assessment of the L1-5Ah anode (left) and cathode (right).....	26
Figure 21: Swollen L1-5Ah pouch cell with visible sensor trace damage.....	26
Figure 22: Opened L1-5Ah pouch cell with direct view on the integrated L1 sensor unit.....	27
Figure 23: Cell stack thickness comparison. 'Swollen' stack side where sealing area was located (left) vs. opposite stack edge (right).....	27
Figure 24: Damaged anode sheet with 'swollen' active material sections in wave-shape (left) and cathodes in good condition without any abnormalities (right).....	27
Figure 25: Schematic drawing of a L1-5Ah pouch cell with double layer pouch foil.....	28
Figure 26: Production process of L1-5Ah pouch cell with double layer pouch foil.....	29
Figure 27: Testing facility.....	31
Figure 28: Nail penetration test of 1 Ah baseline cell.....	33
Figure 29: Nail penetration test of 1 Ah cells with integrated Level-2 sensors.....	33
Figure 30: Chronological sequence: cell before nail penetrates (left), nail penetrated the cell (middle), thermal runaway (right).....	34
Figure 31: 1 Ah baseline, Level-1, and Level-2 sensor cells during and at the end of the heating test.....	35



Figure 32: Heating test on baseline cell (1 Ah).....	35
Figure 33: Heating test on cell with Level-1 sensor (1 Ah).....	36
Figure 34: Heating test on cell with Level-2 sensor (1 Ah).....	36
Figure 35: Overcharge test on baseline cell (1 Ah) and cell with Level-2 sensor (1 Ah); Cells with Level-2 sensor provide additional information on the reference voltage (LFP) vs. Anode.....	37
Figure 36: Sample pictures of the videos documenting the Overcharge test on baseline cell (1 Ah) and cell with Level-2 sensor (1 Ah).	38
Figure 37: Quantitative results yielded from SOH estimation algorithm for baseline cells.	39
Figure 38: Output of SOS algorithm for overcharge test (Baseline Cell): Overall SOS, SOS by terms, warning level and triggered alarms. Orange shadowed part represents thermal runaway event.....	40
Figure 39: Pressure vs SOH relationship obtained from the measurement data of cell #3 (Dataset 3.2).	41
Figure 40: RMSE results with different tuning parameters λ_1 and λ_2 for the cost function J for cell #3 (Dataset 3.2).	42
Figure 41: Data recorded in Performance Test #1 (Cell #4, Dataset 3.2): current, voltage, temperature and pressure.....	43
Figure 42: Output of SOS algorithm for Performance Test #1 (Cell #4, Dataset 3.2): Overall SOS, SOS by terms, warning level and triggered alarms.	44
Figure 43: Calculated voltage responses of the anode (red curve) and cathode (yellow curve) (both versus an ideal 0V reference), as well as the measured cell voltage (blue curve) for the Hybrid Pulse Discharge test.	45
Figure 44: Comparison of measured and simulated voltage responses of the overall cell and respective electrodes (versus an ideal 0V reference) with the original parameter estimation procedure. The measured anode and cathode voltage curves (blue) were NOT used in the parameter estimation routine.	46
Figure 45: Comparison of measured and simulated voltage Response of the overall cell voltage and respective electrodes (versus an ideal 0V reference) with an adjusted parameter estimation procedure. The measured anode and cathode voltage curves (blue) were used in the parameter estimation routine.....	46
Figure 46: Module overview.....	48
Figure 47: Module and electrical cabinet.....	49
Figure 48: PMDU - BMS master - BMS slave.....	49



Abbreviations

Symbol / Abbreviation	
AFE	<i>Analog Front-End</i>
ASIL	<i>Automotive Safety Integrity Level</i>
BL	<i>Baseline Cell</i>
BMS	<i>Battery Management System</i>
BOL	<i>Beginning of Life</i>
C_n	<i>Nominal Capacity</i>
DFN	<i>Doyle-Fuller-Newman model</i>
DOD	<i>Depth of Discharge</i>
ECM	<i>Equivalent-Circuit Model</i>
EIS	<i>Electrochemical Impedance Spectroscopy</i>
EOL	<i>End of Life</i>
EUCAR	<i>European Council for Automotive R&D</i>
EV	<i>Electric Vehicle</i>
L1	<i>Level 1 Sensor Unit</i>
L2	<i>Level 2 Sensor Unit</i>
LFP	<i>Lithium Iron Phosphate</i>
LiPF₆	<i>Lithium Hexafluorophosphate</i>
NMC	<i>Nickel Manganese Cobalt</i>
OCV	<i>Open Circuit Voltage</i>
PCB	<i>Printed Circuit Board</i>
PLC	<i>Programmable Logic Controller</i>
PMDU	<i>Power Management Distribution Unit</i>
PP	<i>Polypropylene</i>
RMSE	<i>Root-Mean-Square Error</i>
SOC	<i>State of Charge</i>
SOH	<i>State of Health</i>
SOS	<i>State of Safety</i>
SOX	<i>State of various Parameters (X)</i>
WLS	<i>Weighted-Least-Square</i>
WP	<i>Work Package</i>
XPS	<i>X-ray photoelectron spectroscopy</i>



1 Introduction

The document titled "Test Report on Cell and Module Performance and Safety", reflects the activities conducted within the framework of Task 5.1, specifically focusing on the "Validation Testing of Cells and Modules" developed in the SENSIBAT project. This report encapsulates the outcomes derived from the testing procedures and analyses their alignment with the objectives of the SENSIBAT initiative.

The results mentioned in this document are, on the one hand, the results of the entire test scope of the manufactured baseline cells, cells with incorporated L1 and L2 sensor units as well as the produced demonstrator module. and on the other hand, the validation of the developed algorithms for cells equipped with L1 and L2 sensors as well as for the demonstrator module. Ranging from the performance tests, long-term behaviour evaluations (calendar life, cycle life), electrochemical impedance spectroscopy (EIS) results, pulse discharge (DCH) and drive-cycle analyses, and post-mortem examinations. Additionally, the document delves into the critical realm of safety, presenting information on performed safety tests, including the nail penetration test, heating test, and overcharge test.

In addition, the taken considerations with respect to the storage, distribution, analysis and interpretation of the recorded cell and sensor data are shown in this document.

In summary, this document serves as a comprehensive repository of insights and analyses derived from the exhaustive validation testing efforts conducted within the SENSIBAT project.



2 Testing Plan

In this section, the reference to the submitted report D1.2 “Testing plan for cells and modules” [2] is explained, and how these two documents relate to each other.

The document D1.2 “Testing plan for cells and modules” defines all tests which must be conducted within the SENSIBAT project on cell and module level to enable an in-depth evaluation of the influence of the integrated sensors on the operational parameters, which serves proper validation of the SENSIBAT sensor, cell, and module development.

The structure of this document was closely based on the structure of D1.2 [2] to ensure comparability of the results that had to be developed in the SENSIBAT project.

As described in D1.2 not every test on cell and module level was completely defined at the project start phase, but specifically developed during the project as those tests are not for comparison among cells but rather for finding operational strategies for sensor-based cells only. Also, during the project unexpected circumstances arose which led to the fact that the overall test and shipment schedule, for cells with and without incorporated sensors as well as for the module, was slightly changed. All partners involved always tried to adapt the upcoming test procedures according to the actual project circumstances in order to be able to achieve the project goals in the best possible way. These circumstances also led to the fact that the tests and shipments carried out partially deviated from the planned testing and shipment schedule (defined in D1.2 [2]). The same applies to the actual number of produced and tested cells.

Following sections present the results and elaborated insights of the conducted tests and which special consideration has been given to store, analyze, compare, and interpret data:

- Performance Test
- EIS
- Calendar life test
- Cycle life test
- Pulse-discharge test
- Drive-cycle test
- Safety test
- Module component test



3 Data Storage for Result Analysis

Due to the larger amount of data expected compared to a scenario without sensor-integrated cells, as well as the amount of test performing partners, special consideration has been given to data aspects such as data storage, analysis, compression, metadata/descriptors, correlation, and combination with other data. A shared folder was organized where all involved testing partners were able to upload and access relevant data. The following information was stored on the shared folders during the project and was thus accessible to the entire project consortium:

- Raw data baseline cells (1 Ah and 5 Ah format)
- Raw data L1-pouch cells (1 Ah and 5 Ah format)
- Raw data L2-pouch cells
- Post-mortem data
- Pressure test data interpretation
- Electrochemical performance data interpretation of various tests
- Testing and shipment overview

This way of data management enabled proper sharing, analysis, comparison, and interpretation of the gained information within the project consortium. The provided data was not only used for analysis on cell level but also for state algorithm development on cell (L1 and L2 state algorithms) and module level.

The raw data obtained during the project and its processed results and insights can be made available in redacted form if required for research purposes.



4 Cell Testing and Validation

In this chapter, all tests performed at cell level are presented, and the results are interpreted and validated. Moreover, the influence of sensor implementation on the electrochemical performance is explained.

All the tests presented below have the goal of enabling an in-depth evaluation of the influence of the integrated sensors on the operational parameters of the cell. Each individual test highlights different aspects and all elaborated insights together deliver a profound holistic understanding about the cells with integrated sensing functionalities for smart battery systems.

4.1 Performance Test

The Performance Test were carried out on all types of cells and its aim was to determine the main performance parameters throughout the lifetime of the cells. The obtained results clarify if the integrated sensors have an influence on cell performance and if yes, quantify the respective impacts.

The test procedure starts with a check-up phase where basic operation values of the cells are determined. The test also includes a subsequent 'Capacity and Energy' and 'Power and Resistance' part. The aim of the 'Capacity and Energy' aims to determine the capacity and energy output of the cells and the 'Power and Resistance' provides insights about the internal cell resistance by applying defined charge and discharge pulse phases at certain SOC (State of Charge) levels. Please refer to the deliverable D1.2 "Testing plan for cells and modules" [2] where a detailed test procedure description can be found.

Figure 1 shows a potential and current curve of a conducted Performance Test on a baseline 5 Ah pouch cell.

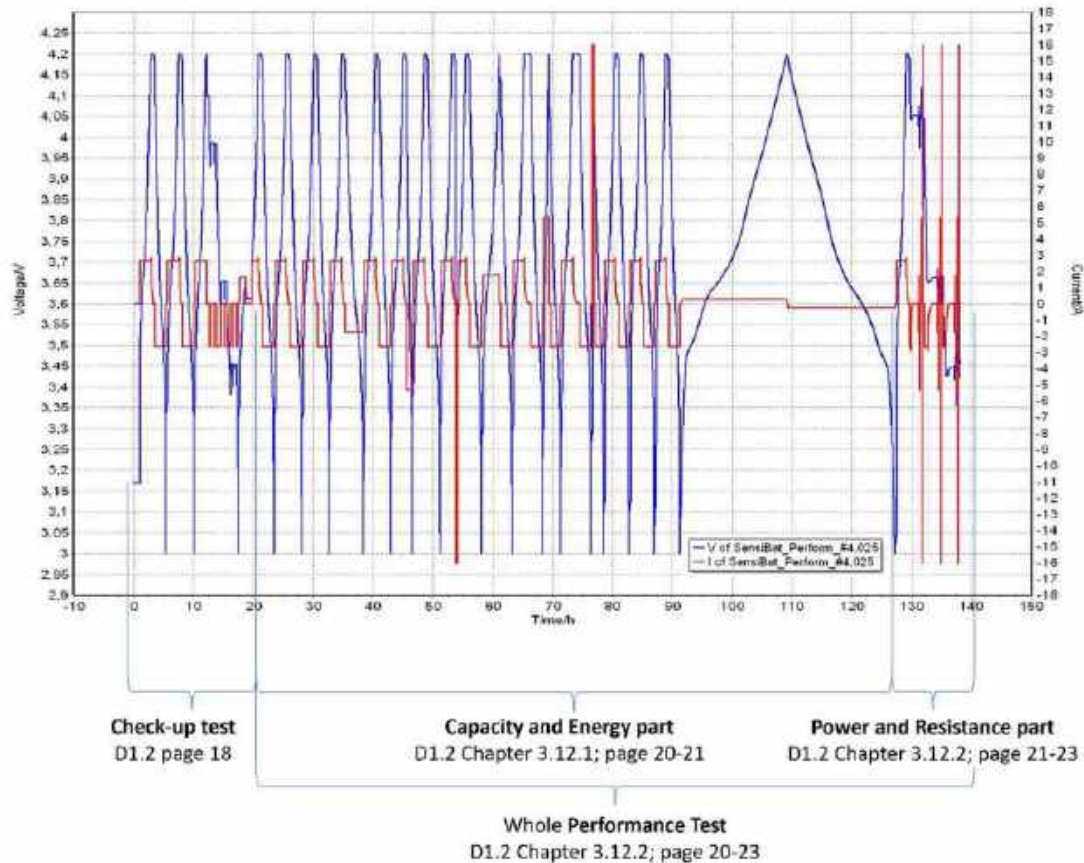


Figure 1: Conducted Performance Test on a baseline 5 Ah pouch cell.



To properly assess the influence of the incorporated L1 and L2 sensors on the overall cell performance, the Performance Test results of following cell systems where analysed:

- BL-5Ah vs. L1-5Ah
- BL-1Ah vs. L1-1Ah vs. L2-1Ah

The following section compares the electrochemical performance and internal resistances of BL and L1 pouch cells in a 5 Ah cell format as overall performance indicators and serves as validation of the integration of the developed SENSIBAT L1 sensor units.

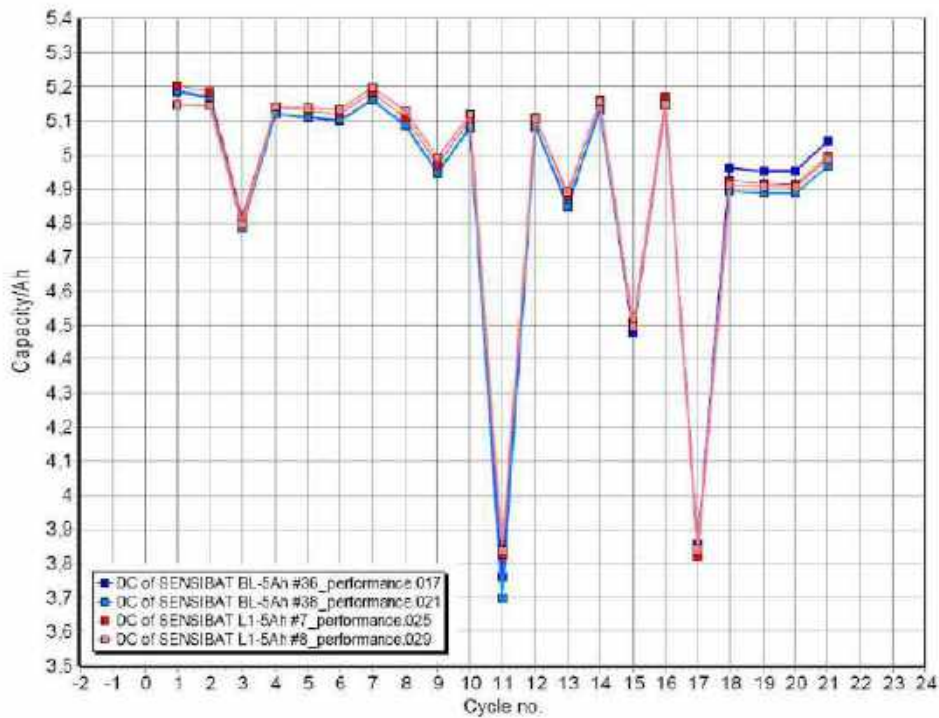


Figure 2: Capacity over cycles comparison of BL-5Ah and L1-5Ah pouch cells. This corresponds to the “check-up” & “capacity and energy” part of the Performance Test.

The visualized capacity values in Figure 2 show that there is no significant difference between the BL cells and the cells with integrated L1 sensors. The small offset between the capacity values of the different cells is correlated to the semi-automatic, pilot scale cell production.

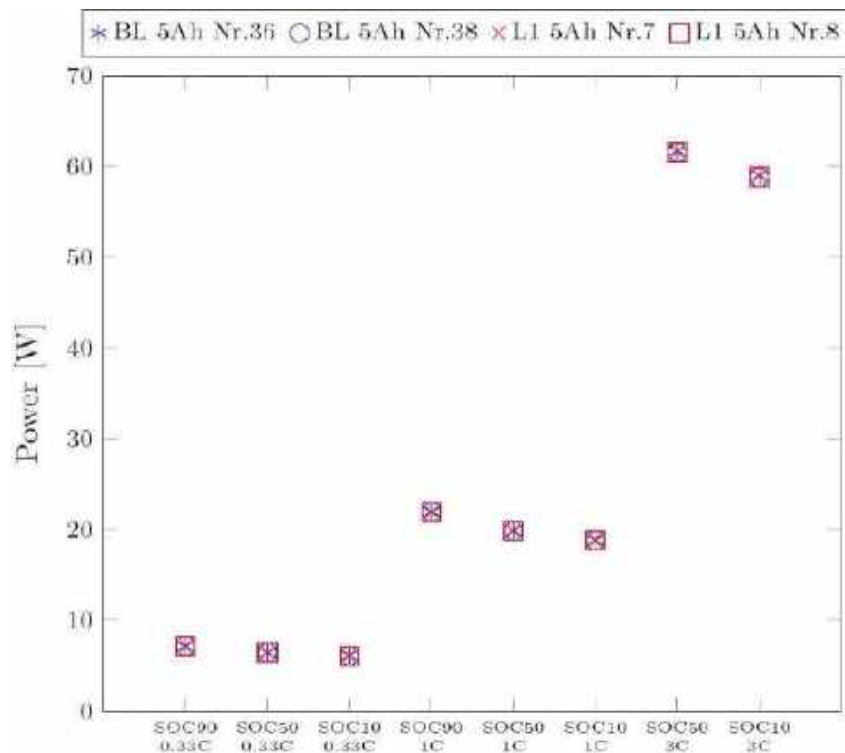


Figure 3: Power during charging of BL-5Ah and L1-5Ah pouch cells at three different SOC levels for three different C-rates. This corresponds to the “power and resistance” part of the Performance Test.

At the “power and resistance” section of the Performance Test specific (dis)charge pulse (constant current) with a duration of 10 seconds was applied using three different C-rates and three different SOC levels. The calculated power is shown for the two BL-5Ah pouch cells and two cells with integrated L1 sensors (L1-5Ah) in Figure 3. The biggest difference between these values of the four different cells at the same SOC and same C-rate is 0.22%. This indicates that the integration of the L1 sensor matrices does not have a significant influence on the electrochemical performance of the cells.

The following section compares the same performance indicators as above but with BL and L2 pouch cells in a 1 Ah cell format and serves as a validation of the integration of the developed SENSIBAT L2 sensor units in a 1 Ah cell format. It must be mentioned that the L2 sensor units were only developed for 1 Ah pouch cell formats according to D1.2 “Testing plan for cells and modules” [2]. Correspondingly, the validation of the L2 sensor unit implementation was conducted by processing 1 Ah pouch cell test data.

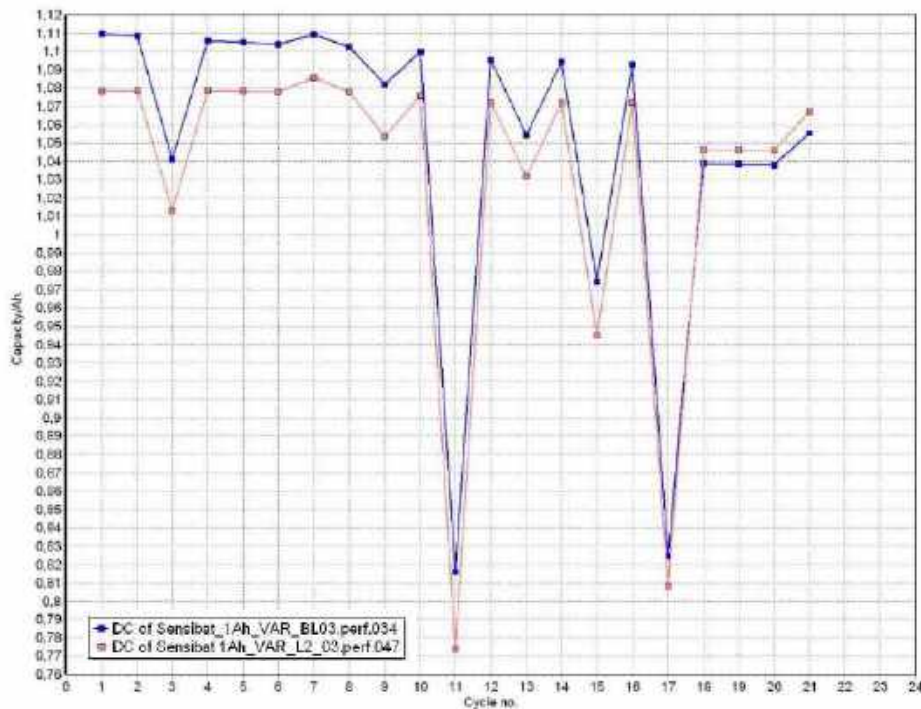


Figure 4: Capacity over cycles comparison of BL-1Ah and L2-1Ah pouch cells. This corresponds to the "check-up" & "capacity and energy" part of the Performance Test part.

Figure 4 shows the discharge capacity values of the tested BL-1Ah and L2-1Ah pouch cells. The absolute deviation in the first discharge capacity values of the "check-up" part between the compared cells is less than 3%. After performing the "capacity and energy" part of the test, where C-rates up to 3C were applied, the L2-1Ah pouch cell delivers higher discharge values than the baseline, which implies a lower fading behaviour. The measured deviation between the capacity values of the different cells is correlated to the semi-automatic, pilot scale cell production.

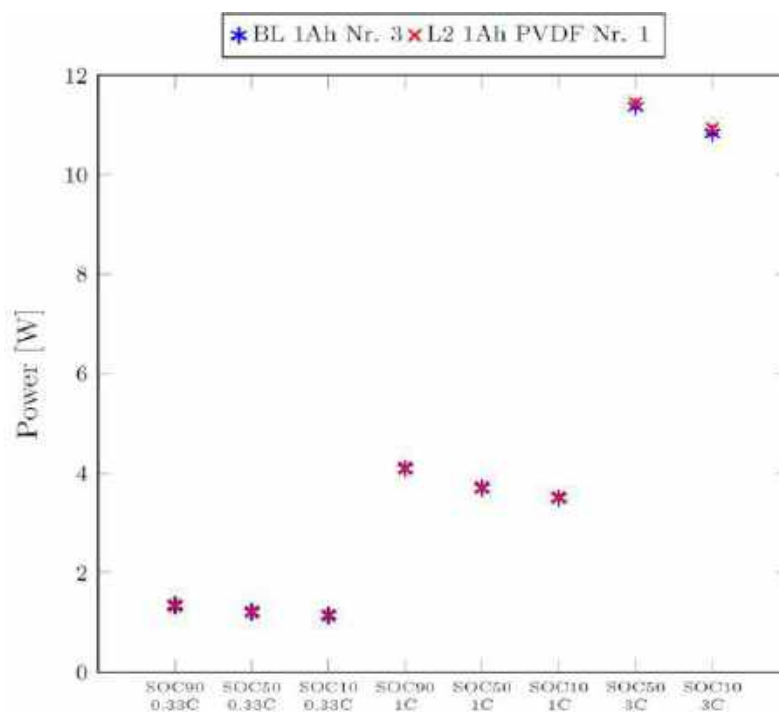


Figure 5: Power during charging of BL-1Ah L2-1Ah pouch cells at three different SOC levels for three different C-rates. This corresponds to the "power and resistance" part of the Performance Test.



The calculated charge power values for BL-1Ah and L2-1Ah pouch cells are shown in Figure 5. The maximum difference between these values of the cells at the same SOC and same C-rate is 0.35%. This indicates that the integration of the L2 sensor units does not have a significant influence on the electrochemical performance of the cells.

4.2 Calendar Life, Cycle Life, (long-term behaviour)

This section delves into critical aspects of the SENSIBAT project, focusing on the cycle-life and calendar-life performance of the developed cells, without and with SENSIBAT L1 and L2 sensors. The objective is to analyse if the developed and implemented SENSIBAT sensors have any impact on the long-term behaviour of the lithium-ion cells. The comprehensive testing procedures, designed to assess the robustness and longevity of the cells under different conditions, were introduced in the deliverable D1.2 "Testing plan for cells and modules" [2].

A Cycle-life test scrutinizes the endurance of the cell through an intricate sequence of steps, including thermal equilibrium, Performance Testing, and cyclic loading. The cumulative cycles from both ageing and Performance Tests contribute to a holistic understanding of the cell's behaviour. The evaluation criteria at the end of 500 cycles or a capacity retention of less than 80% ($C < 0.8C_n$) guide the decision-making process, ensuring a thorough examination of the cell's cycle life in an EV application.

In a similar way calendar life shifts the focus to prolonged storage conditions and the influence of SENSIBAT sensors without cycling. The procedure involves Performance Testing, setting the State of Charge (SOC), and storing the cell under extreme environmental conditions (55°C). The test concludes based on predetermined criteria of 12 weeks or a capacity retention of less than 80% ($C < 0.8C_n$), shedding light on the impact of extended storage and environmental factors on both cell and sensor performance.

The SENSIBAT project made significant advances in the evaluation of the L1-5Ah cells, undergoing rigorous testing through three L1-5Ah cells under cycle-life analysis and two L1-5Ah cells under calendar ageing. It is important to clarify that cells #3 and #4 (Figure 6 and Figure 7, capacity and internal resistance evolution, respectively) have been subjected to cycling with a pressure setup (Figure 9), revealing promising outcomes compared to those without the pressure jig (Cell #1 in the Figure 6 and Figure 7)).

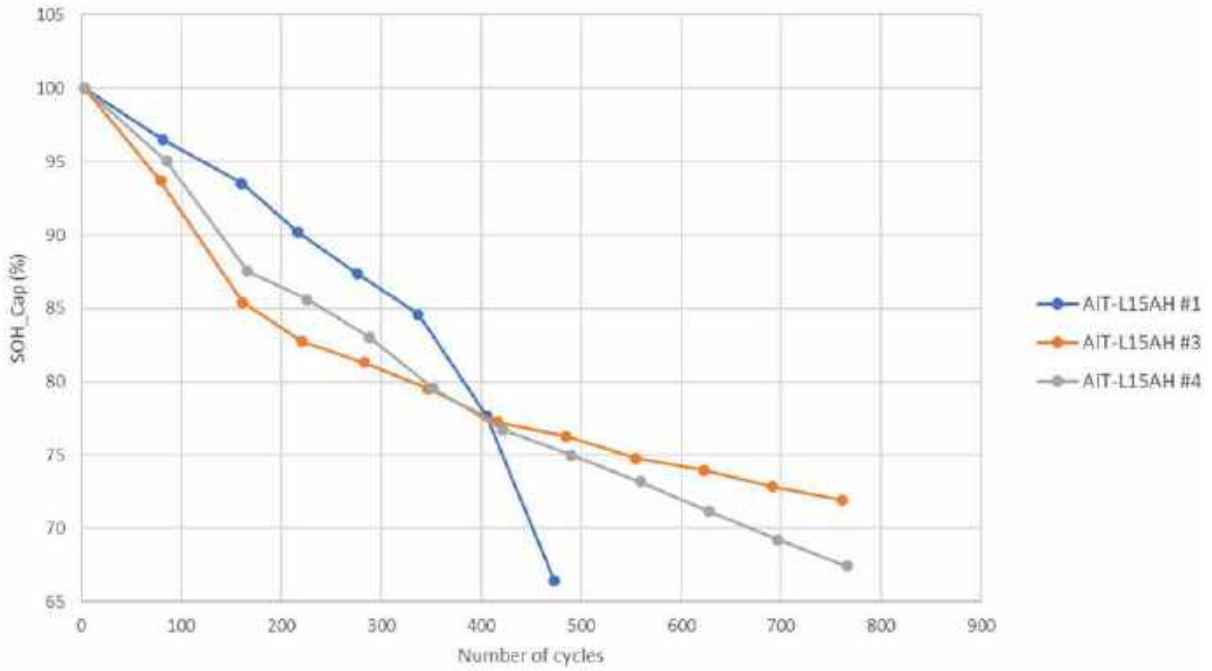


Figure 6: Capacity evolution over cycles in three L1-5Ah pouch cells.

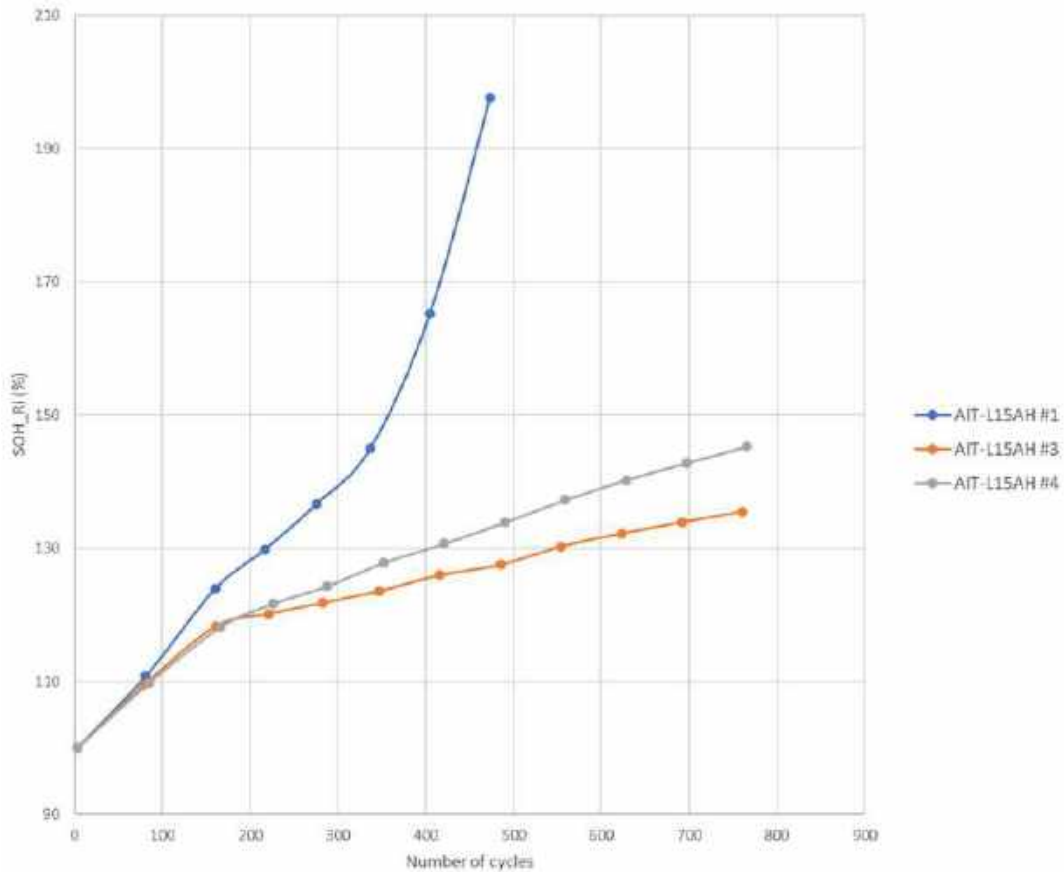


Figure 7: Internal resistance evolution over cycles in three L1-5Ah pouch cells.

After completing 400 cycles, it became evident that the three cells had proceeded below 80% State of Health (SOH), EOL criteria for EV application. Notably, the cell without an applied pressure (cell #1) exhibited a significantly faster rate of internal resistance degradation compared to its counterparts over the same cycle



count. In contrast, the cells with a pressure jig demonstrated enhanced durability, achieving an impressive 750 cycles with a linear ageing trend at 45°C, 100% DOD and 0.5C. The initial stages of this extended cycling period saw a 15% capacity loss and an increase in internal resistance within the first 150 cycles, providing valuable insights into the long-term performance dynamics of the cells under varying conditions. These findings underscore the critical role of pressure application in mitigating degradation and enhancing the overall longevity of the cells in the SENSIBAT project.

Upon concluding the cycle-life testing phase, it was observed that the performance of the L1-5Ah cell and the BL-5Ah cell (without sensor) exhibited remarkable similarity in both capacity and internal resistance evolution (Figure 8, excluding the cell #1 without pressure jig). Notably, the L1 sensor demonstrated no discernible impact on the cycle ageing of the SENSIBAT cells. These findings suggest a parity in performance between the L1 and baseline cells, implying that the introduction of the L1 sensor did not adversely affect the cycle-ageing characteristics of the SENSIBAT cells under the given testing conditions. This alignment in performance underscores the potential compatibility and effectiveness of the L1 sensor, providing valuable insights into the overall robustness and resilience of the cells in the presence of this sensor technology.

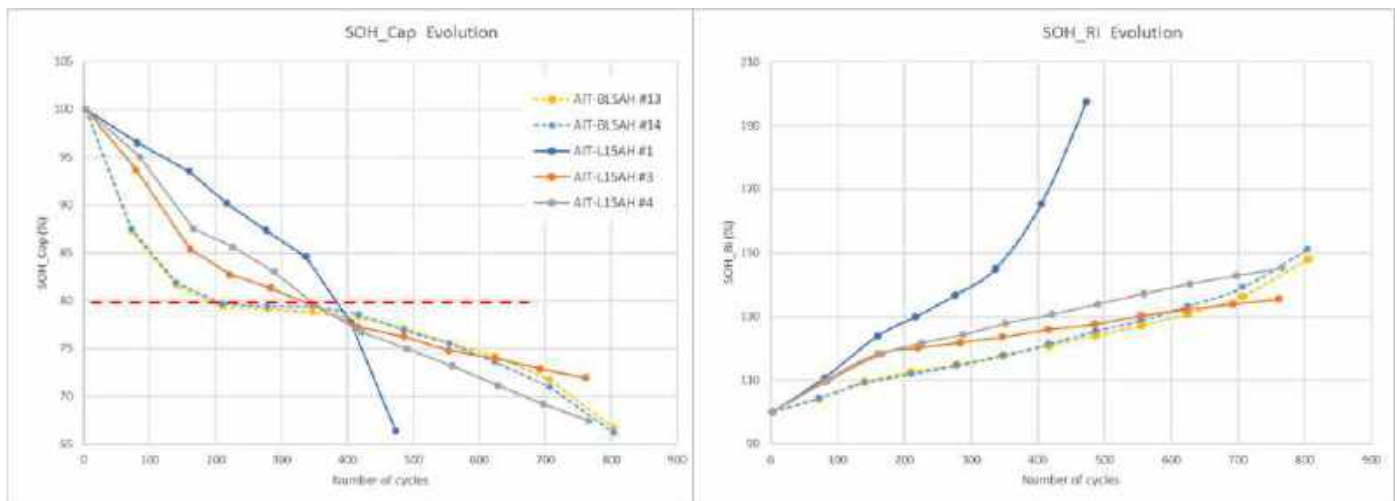


Figure 8: Capacity and internal resistance evolution over cycles in three L1-5Ah pouch cells and two BL-5Ah cells.

As mentioned before, L1-5Ah cells #3 and #4, were subjected to cycling with an external pressure measurement setup (Figure 9), serving a dual purpose. Firstly, this setup was employed to validate the measurements obtained from the L1 sensor, ensuring accuracy and reliability in the collected data. This validation step contributes to the overall confidence in the developed sensor technology and their integration into the SENSIBAT project. Secondly, the use of an external pressure measurement setup was identified as a risk mitigation activity. In the event of L1 sensor damage or unavailability of the readout circuit, the external pressure measurement setup serves as a fail-safe mechanism, allowing continued monitoring of crucial parameters during the cycling process. This strategic approach underscores the project's commitment to ensuring data integrity and reliability, even in the face of potential sensor-related challenges. In fact, the measurements using the external pressure sensor were exploited in the SoX algorithm development as described in deliverable D4.4 [5], whose results will be summarized in chapter 5.

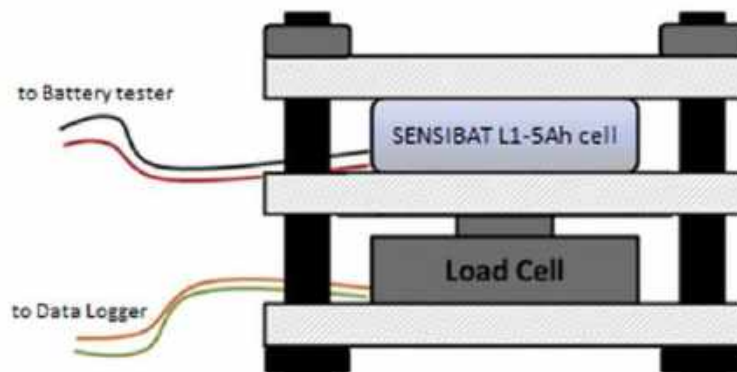


Figure 9: Details of the external pressure measurement setup for L1-5Ah cells.

Indeed, a noteworthy challenge has surfaced as all cells experienced electrolyte leakage from the sensor feedthrough area. This observation, explained in detail in the 4.5 section, underscores the importance of external pressure measurement.

Regarding the calendar-life tests, a deviation from the initial testing plan (D1.2 [2]) was introduced after the tests with the BL-1Ah, the cells were below 80% SOH after only 2 weeks at 55°C. After these first results, the cells were aged with a calendar condition set at 45°C and 100% State of Charge (SOC), deviating from the planned 55°C.

Figure 10 and Figure 11 show that after a month (30 days) under these new conditions, similar results were observed in both BL-5Ah (cell #10) and L1-5Ah cells (cells #5 and #6). However, a notable discrepancy emerged as only one out of the five tested cells, specifically BL-5Ah cell #10, remained functional after 40 days at 45°C and 100% SOC. This outcome introduces complexity into the conclusion regarding the absence of an impact from the L1 sensor on the calendar ageing of SENSIBAT cells. The challenging conditions imposed, characterized by both elevated temperature and maximum SOC, show up the aggressiveness of the testing environment and its potential influence on the cells' long-term performance. These findings demand a re-evaluation of the



interaction between the L1 sensor and the dynamics of calendar ageing, emphasizing the importance of a discerning interpretation due to the dual impact of challenging conditions on the cells.

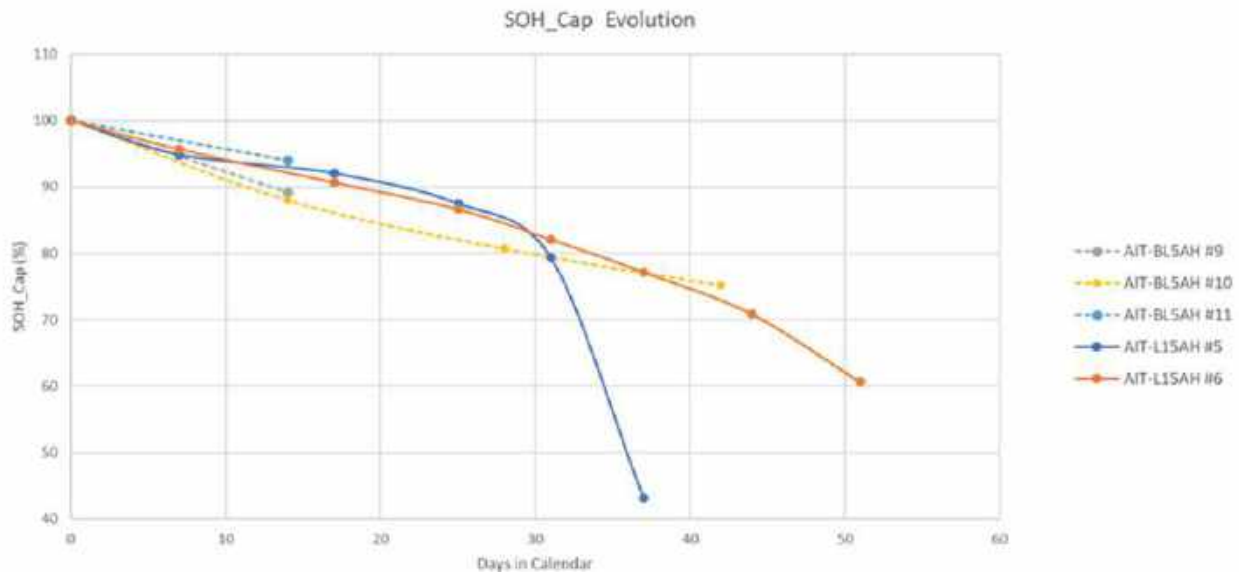


Figure 10: Capacity evolution over time in two L1-5Ah pouch cells and three BL-5Ah cells.

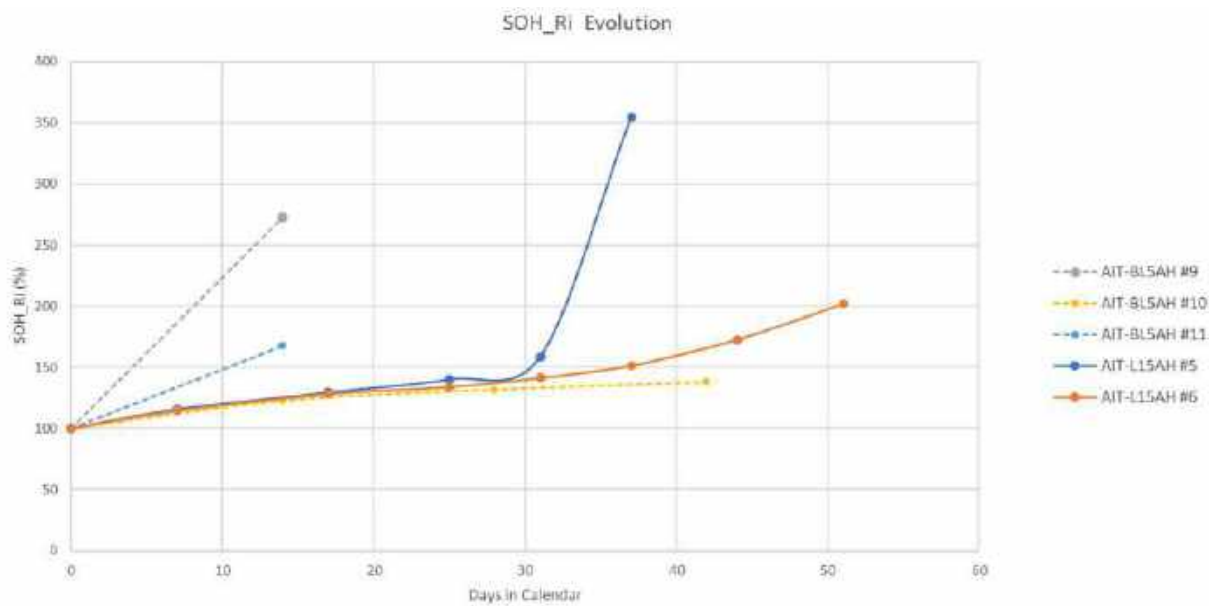


Figure 11: Internal resistance evolution over time in two L1-5Ah pouch cells and three BL-5Ah cells.

Consistent outcomes were observed in both the cycle- and calendar-life evaluations of L2-1Ah cells, featuring the integration of the third electrode. The testing protocols revealed comparable performance trends under cycle ageing between baseline and cells with sensors, underscoring the stability of the cells and sensors under diverse conditions (with and without sensors). This congruence in results further strengthens the absence of sensor influence on cell cycle-life, regardless of the used sensor, L1 and L2. Such uniformity in performance across different phases of testing lends support to the reliability and robustness of the SENSIBAT project's cells and sensors. Furthermore, it is crucial to note that the same conclusions cannot be drawn for calendar ageing. During the assessments, the cells exhibited premature degradation both with and without the sensor, which can be attributed to highly aggressive ageing conditions. Thus, caution must be exercised in extending the conclusions drawn from cycle-life evaluations to calendar-life scenarios within the context of the SENSIBAT project.



4.3 EIS Results

EIS measurements were conducted in order to have an additional evaluation method to validate the influence of the integrated L1 and L2 sensors on the cell performance, by measuring the impedance of the cells at different SOC levels and applying a certain frequency range according to the specific test requirements given in D1.2 [2]. The EIS result examines the response characteristics of the tested cell to the frequency range of interest, which can be used as an indicator of cell performance. The EIS test was conducted right after the Performance Test and not after the long-term testing (Cycle Life and Calendar Life testing).

Figure 12 shows the Nyquist plot of a BL-5Ah and L1-5Ah pouch cell. The impedance deviation of the two measured cell types is so small that it can be assumed the pilot line production process tolerances impact cause the obtained reproducibility values. and is within the tolerance. This data is in line with the results from Chapter 4.1. and has proven that the integration of sensor units does not have an impact on the short or middle-term cell performance.

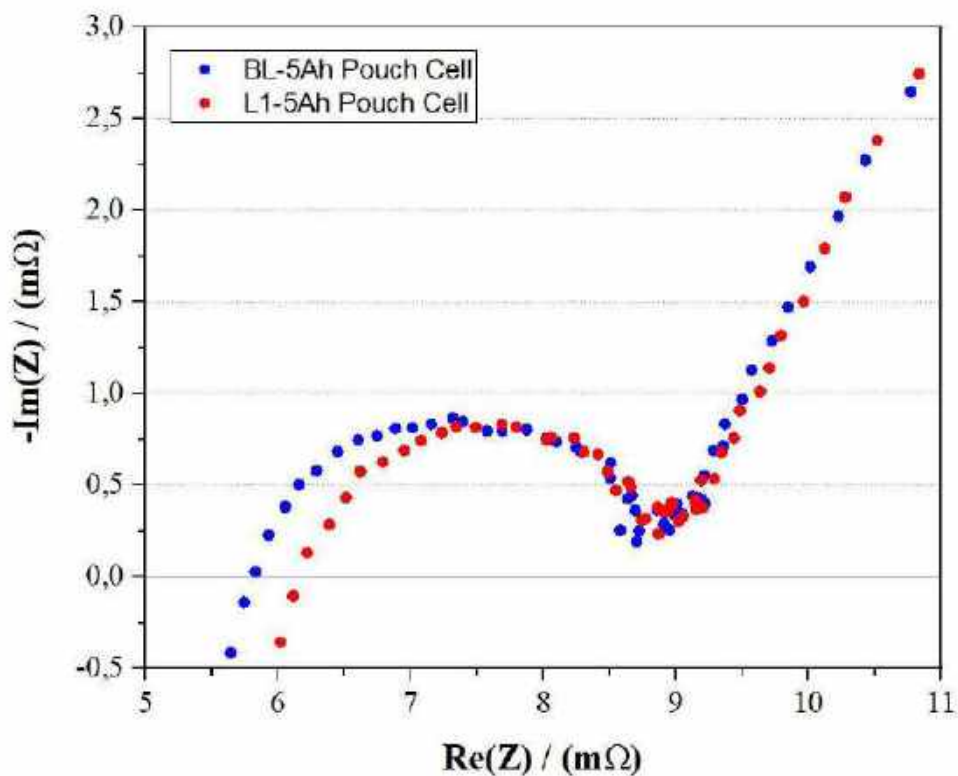


Figure 12: EIS plot of BL-5Ah pouch cell vs. L1-5Ah pouch cell.

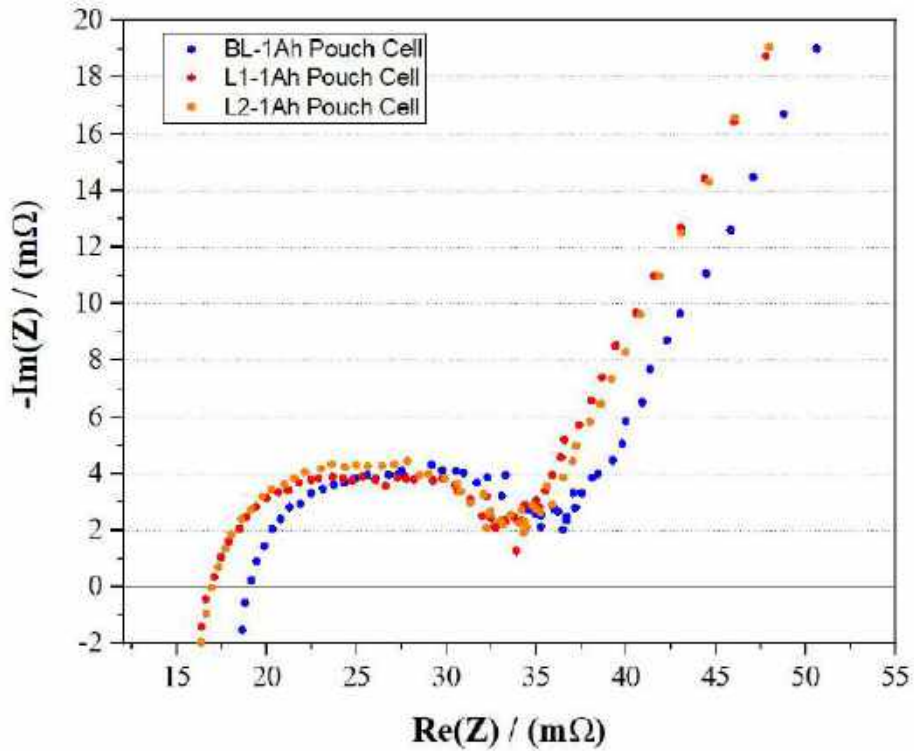


Figure 13: EIS plot of BL-1Ah pouch cell vs. L1-1Ah pouch cell vs. L2-1Ah pouch cell.

Figure 13 shows the measured complex resistance of the 1 Ah prototype cells in a BL, L1 and L2 cell configuration. Comparable to the 5 Ah cell data analysis, it can be concluded that the integration of the developed sensor units (L1 and L2) does not have an influence on the complex resistance of the cells at certain frequency ranges.



4.4 Pulse DCH, Drive-cycle

Additional tests were conducted with L2-1Ah pouch cells to deliver valuable data, particularly OCV, current and reference potential (LFP vs. Gr) and how these variables correlate with each other. These values were processed and interpreted for advanced L2 state estimation algorithms development, the results of which were described in detail in D4.5 [6], the summary of which is described in chapter 5. Therefore, a pulse-discharge cycle and a drive-cycle test protocol was programmed and subsequently conducted with the fabricated L2-1Ah pouch cells. Accuracy of the obtained L2-reference electrode response on the applied charge and discharge pulses was of high importance with respect to the aimed state estimation algorithm development.

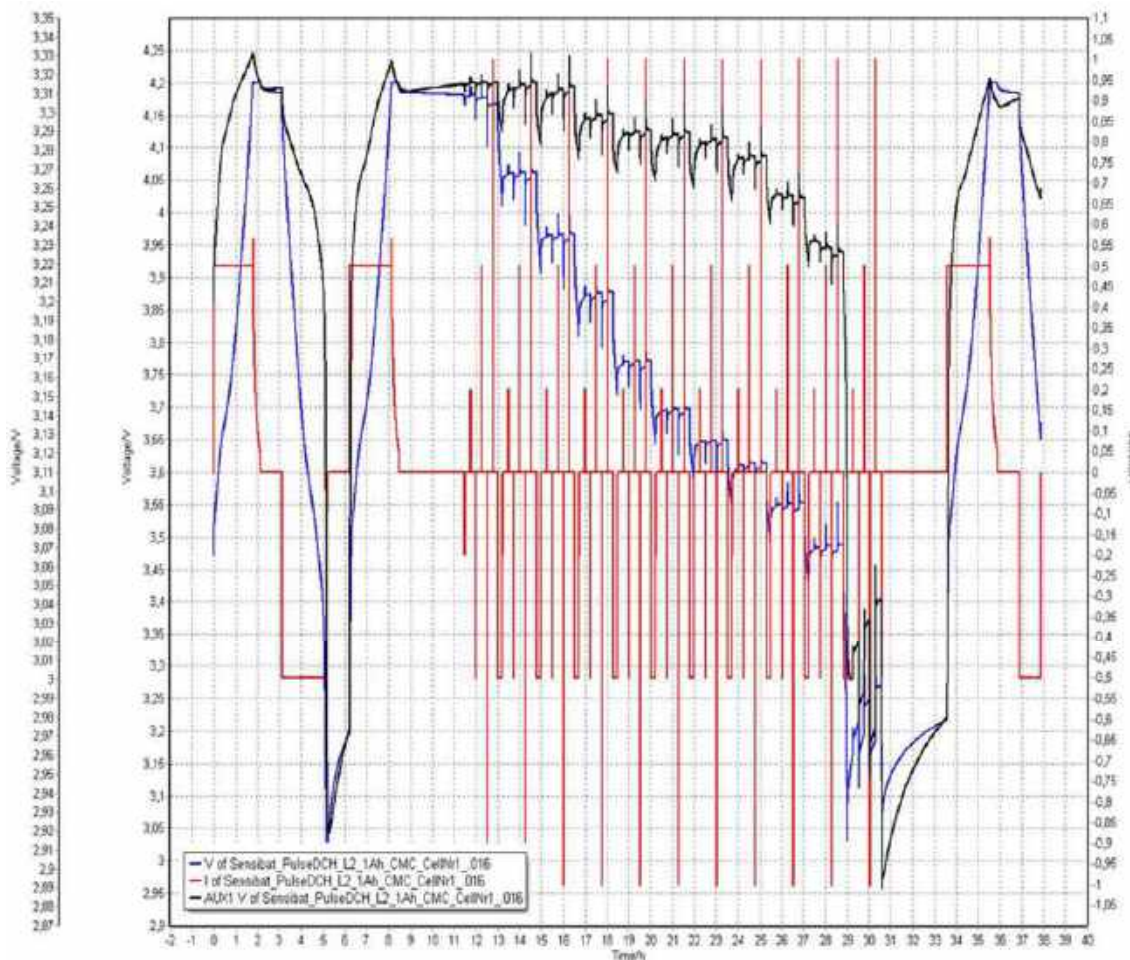


Figure 14: Current (red, right-hand-side y axis), cell voltage (blue, voltage y-axis up to 4.25V) and reference potential (LFP versus graphite; black, voltage y-axis up to 3.35V) for a pulsed discharge test.

Figure 14 shows the cell potential and current curve as well as the measured reference potential (LFP vs. Gr.) of the conducted discharge pulse test. The test starts with a charge-discharge-charge cycle, after which the battery is discharged in steps. After each discharge step, the voltage relaxes, and the end point is taken as Open-Circuit Voltage (OCV) point versus the SoC at that point. The latter value is obtained by Coulomb counting. Moreover, Hybrid Pulses tests are performed at the end of relaxation. The accuracy of the reference potential response to the applied current was as good as expected. The correlation between the measured OCV, applied current and additionally tracked reference potential was a useful input parameter for L2 state estimation algorithms development as described in detail in D4.5 [6]. A summary is given in chapter 5.

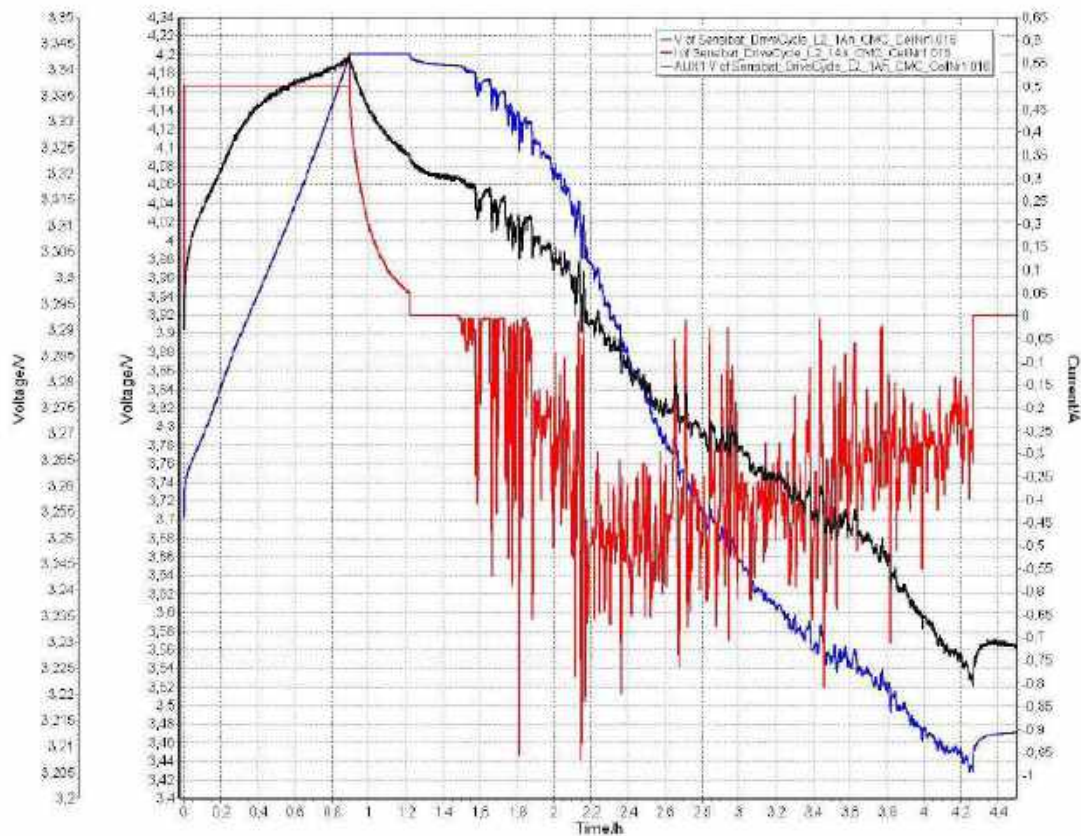


Figure 15: Current (red), cell voltage (blue) and reference potential (LFP versus graphite; black) for a drive-cycle test.

A specific drive-cycle test was programmed and conducted to apply a more realistic stress profile to the cells and to allow parametrization of a physics-based model as described in D4.5 [6]. The received results are better representing actual driving behaviour. The obtained values (shown in Figure 15) confirm the above-mentioned good reference potential response to the applied current. Here again, the correlation between the measured OCV, applied current and additionally tracked reference potential (LFP vs. Graphite) was used as an additional input for L2 state estimation algorithms development. More detailed information about the conducted state estimation algorithms and their validation can be found in chapter 5.

4.5 Post-mortem Analysis

This section provides results of the conducted post-mortem analysis of the cells and the derived insights. The main aim was to detect chemical and physical differences between cycled BL, L1 and L2 pouch cells. The particular cells were formed and tested according to the testing plan.

Figure 16 shows the cathode (left), anode (middle) and the separator (right) of a disassembled BL-5Ah pouch cell which underwent the cycle life test.



Figure 16: BL-5Ah pouch cell post-mortem components including cathode (left), anode (middle) and separator sheet (right).

The BL-1Ah and L1-1Ah cells were also opened after testing to assess the integrity of individual cell components. Figure 17 shows the extracted anode and cathode of a BL-1Ah cell inside an argon-filled glovebox. The electrodes show no visible damage, while the changes in contrast are due to the dried electrolyte.



Figure 17: Visual assessment of the BL-1Ah anode (left) and cathode (right).

Similarly, the electrodes from the L1-1Ah cells, have not shown an out of the ordinary damage to the electrodes, as seen in Figure 18. The white spots are from the LiPF_6 salt from the dried electrolyte, while the delamination of graphite from the Cu current collector is due to the handling of the electrodes after opening them. The lack of the white spots on the BL-1Ah electrodes stems from the fact that the images were taken immediately after opening the cell (in case of BL-1Ah cells) or after some time has passed (in case of L1-1Ah cells), allowing for more thorough drying of the electrolyte.



Figure 18: Visual assessment of the L1-1Ah anode (left) and cathode (right).

Nevertheless, when studied with X-ray photoelectron spectroscopy (XPS), both BL-1Ah and L1-1Ah cells show Ni deposition on the anode, indicating a crosstalk between the electrodes (Figure 19). This is a common issue with NMC-type cathodes and organic electrolytes and may explain the capacity fade with cycling of all the cells.

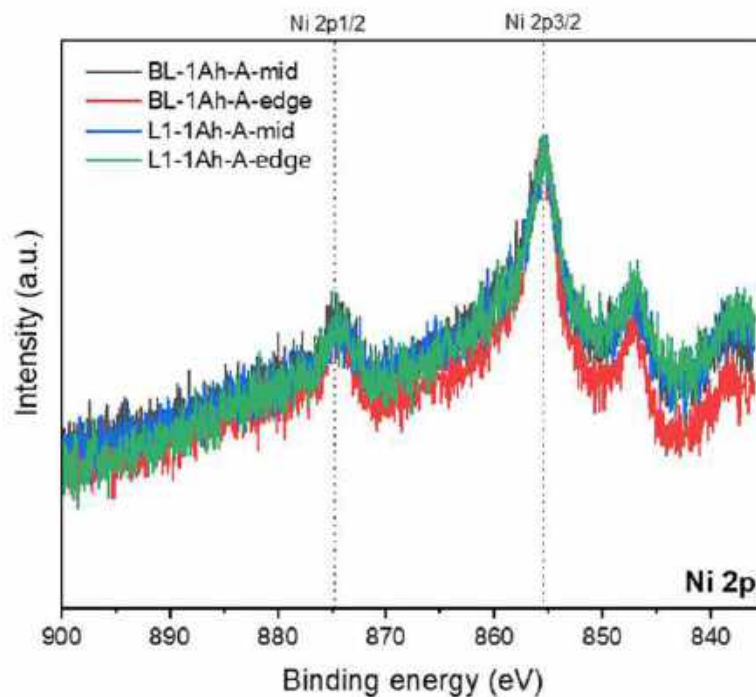


Figure 19: XPS of BL-1Ah and L1-1Ah anodes either from the middle or the edge of the electrodes stack.

On the other hand, L1-5Ah battery cells show a more thorough damage to the anodes, but interestingly not on the cathodes (Figure 20). Furthermore, this damage consists of wrinkles and “burnt” area that coincides with the region where the L1 sensor feedthrough was connecting the inner and outer parts of the cell.



Figure 20: Visual assessment of the L1-5Ah anode (left) and cathode (right).

In order to gain insights about the L1 sensor implementation on the overall cell performance of the produced 5 Ah pouch cells, L1-5Ah pouch cells were also used for a post-mortem analysis. The cells were also cycled (Performance Test and EIS) and afterwards stored for several months in a dedicated battery storage container. This analysis also allowed the long-term effect of the sensor integration to be evaluated.

Before getting the L1-5Ah cells prepared for the subsequent post-mortem analysis, a visual aging effect was determined. The thickness of the cell, especially at the sensor feedthrough area was higher. It seemed that during the months of storage, the cell stack was 'swollen' and 'inflated'. Figure 21 shows the 'swollen' L1-5Ah pouch cell, which was cycled and stored, with visible sensor trace damage (partially dissolved), possibly by the leakage of the electrolyte into the encapsulation. A solid expansion area at the sensor feedthrough cell stack edge was obviously recognizable. Gas formation could be excluded as the swollen area could not be compressed by applying a pressure. An agglomeration of crystallized Li salt or "swollen" active material on the electrodes was assumed to be a possible reason for the increase in thickness.



Figure 21: Swollen L1-5Ah pouch cell with visible sensor trace damage.

After the visual inspection, the cell was transported into a glovebox and a post-mortem analysis was performed under Argon atmosphere in the same way as for the reference sample (BL-5Ah pouch cell). Following image (Figure 22) shows the opened L1-5Ah pouch with the L1 sensor unit. No "eye-catching" failure of the L1 sensor could be detected from visual inspection.



Figure 22: Opened L1-5Ah pouch cell with direct vie on the integrated L1 sensor unit.

The assumption that the increase in thickness was caused by swollen electrodes was confirmed on closer inspection of the electrodes.



Figure 23: Cell stack thickness comparison. 'Swollen' stack side where sealing area was located (left) vs. opposite stack edge (right).

Figure 23 presents the thickness difference between the two cell stack edges. The edge where the L1 sensor feedthrough area was located has a greater thickness. The anodes and cathodes were then analysed individually.



Figure 24: Damaged anode sheet with 'swollen' active material sections in wave-shape (left) and cathodes in good condition without any abnormalities (right).



Figure 24 shows the damaged anode sheet with 'swollen' active material sections in wave-shape (left) and a cathode sheet in good condition without any abnormalities (right). It can be concluded that the L1 sensor integration has a long-term influence on the integrity of individual cell components.

4.5.1 Risk Mitigation

As the evaluation of the long-term behaviour was only carried out at a late stage of the project, it was no longer possible to implement significant changes in terms of cell sealing (components, processes) or sensor layout development. Nevertheless, the SENSIBAT partners focused on finding possible solutions for future sensor integration approaches in the final project phase. Furthermore, AIT has found a way to offer a trade-of solution to produce and deliver 5 Ah pouch cells that do not have electrolyte leakage problems but allow data collection using pressure and temperature sensor units in the final demonstrator module. Figure 25 shows the schematic drawing of the L1-5Ah pouch cell where a BL-5Ah cell serves as a base. The L1 sensor unit was placed on the closed BL-5Ah pouch cell. The whole set-up was finally closed by adding an additional pouch foil layer on top of the L1 sensor unit. The dimensions of the three used pouch foil elements have been changed slightly and adapted in order to have matching, overlapping areas for the sealing process. With this design, it was possible to provide the module construction partner with cells that have both pressure and temperature sensing functionalities integrated and pose no risk of electrolyte leakage. As the pressure is evenly distributed through the pouch film layer, no deviation of the pressure measurement during the cycle was expected compared to the original L1-5Ah pouch cell configuration. The measured temperature values are expected to be slightly affected by the foil layer in between compared to the original L1-5Ah pouch cell configuration.

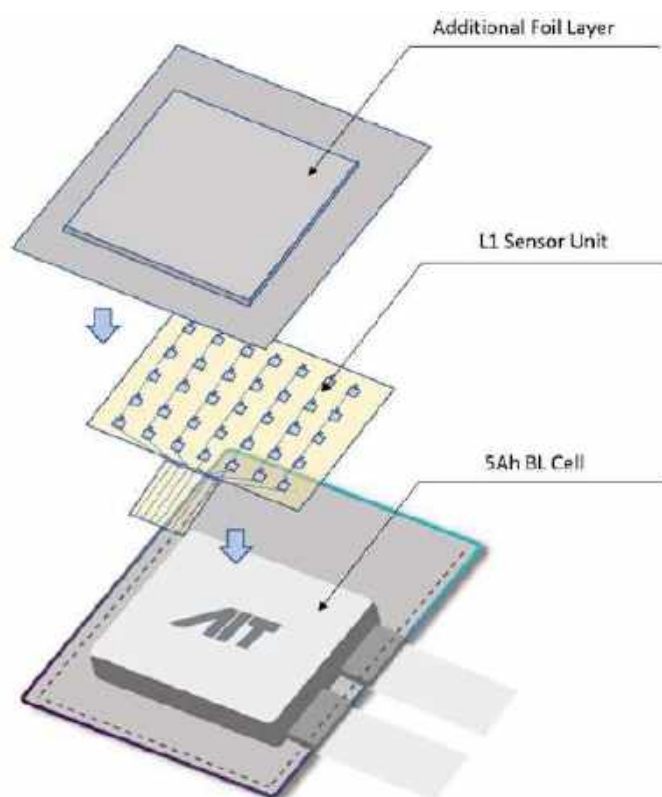


Figure 25: Schematic drawing of a L1-5Ah pouch cell with double layer pouch foil.

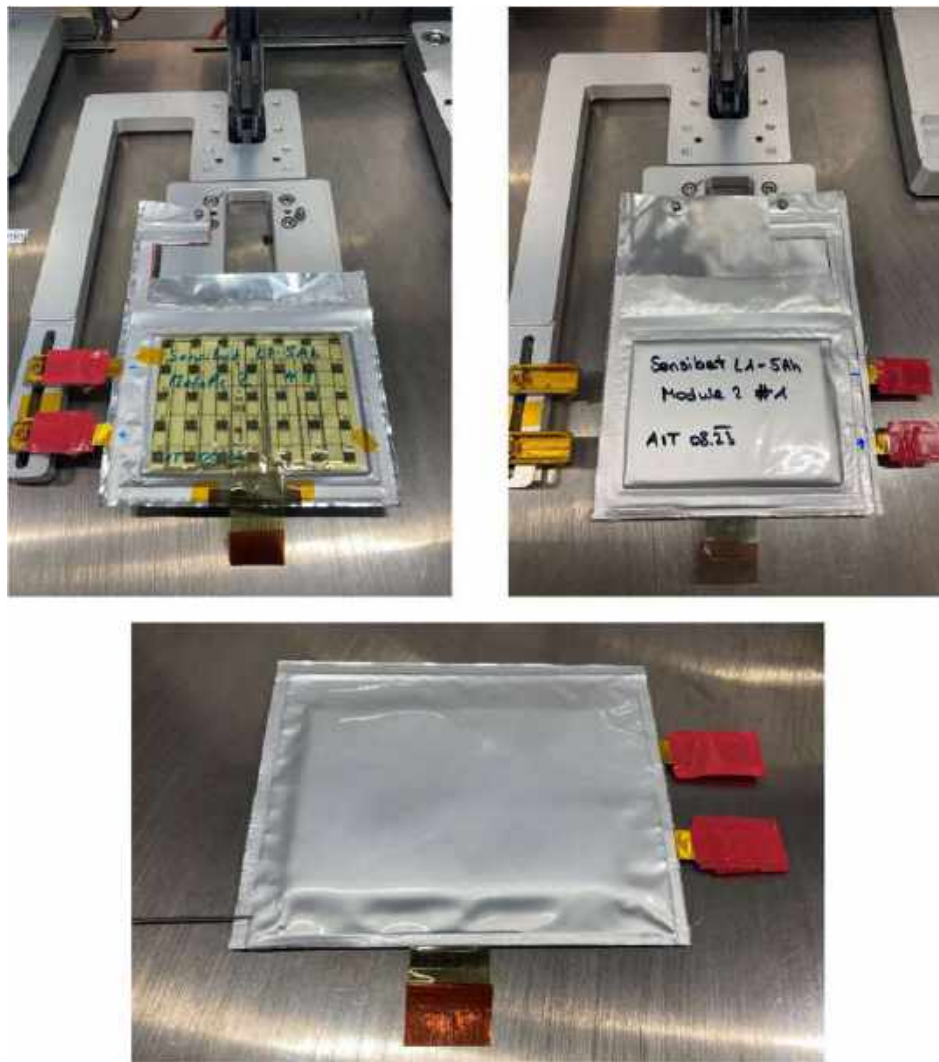


Figure 26: Production process of L1-5Ah pouch cell with double layer pouch foil.

The images above (Figure 26) show the production process of the L1-5Ah pouch cell where an additional foil layer was used.

It can be assumed that the used material combination for the L1 sensor encapsulation (Parylene C) and the melting layer of the pouch foil (PP) does not produce a satisfactory sealing. Once the melting polymer of the pouch foil has solidified, the adhesive forces are not sufficient for a permanently satisfactory sealing.

Assumptions for potential risk mitigation measures for future sensor integration project approaches:

- Adaption of material combination for the sensor encapsulation and the sealing material of the inner pouch foil layer could minimize or even mitigate the issue.
- Furthermore, the use of surface treatment techniques such as roughening the affected surfaces is a possible measure to drastically improve the quality of the sealing.

Ideally, both measures should be analysed in combination in further investigations. This is the best possible solution from today's perspective.



4.6 Safety

The safety tests included baseline, Level-1, and Level-2 sensor cells, with a specific focus on issues encountered with the Level-1 sensor cells. Due to a delay in the project timeline, these cells were stored until month 36 of the project, at which point safety tests were conducted to assess their performance. The storage time of the BL and L1 cells was 20 months and the L2 cells were stored for 8 months. Unfortunately, the storage duration led to minor electrolyte leakage in the Level-1 sensor cells, rendering them unsuitable for thoughtful measurement and comparison in safety tests. The subsequent sections, delve into the specific conditions and outcomes of the performed safety tests, including the Nail Penetration test, Heating test, and Overcharge test. The results provide insights into the thermal and electrical behaviours of baseline cells and those equipped with Level-1 and Level-2 sensors, contributing valuable data to the evaluation of safety aspects within the SENSIBAT project.

4.6.1 Information on the performed Safety Tests

Within D1.2 [2] safety tests for baseline, Level-1 and Level-2 sensor cells were defined. Unfortunately, problems occurred with the Level-1 sensor cells. Since the cells were produced until month 19 of the project (including a 4-month delay as reported in D3.2 [3]), the cells were stored until the safety test were performed. This was done at month 36, as the safety test facility demands cumulated, efficient safety testing due to workload issues. While the initial cycling tests of the cells reported in D3.2 [3] (and prolonged cycling afterwards), displayed that the issues regarding electrolyte leakage at the feed-through were solved, the storage duration obviously resulted in minor electrolyte leakage for the cells containing Level-1 sensors at the sensor sealing area. In consequence, the cells lost their cell voltage and could not be seriously measured and compared in the safety tests. The leakages at the feed-through were further reported by partner AIT when investigating 5 Ah cells with Level-1 sensors. Further information regarding possible causes for this issue as well as a risk mitigation strategy for future projects can be found in chapter 4.5.

For the 1 Ah cells in connection with VAR sealing equipment this leakage seems to occur at a low level during prolonged time, as the electrochemical testing did not reveal unwanted voltage changes / or visual electrolyte loss at the feed-through area.

In the following, the test conditions for the performed tests are described:

- Nail penetration test

The typical sequence for this test is to fix the cell in a housing capable to perform safety tests. In a second step a nail with a diameter of 3 mm is penetrated through the cell with the speed of 80 mm/s. An example for this measurement setup and the robust housing (with suction of gases, etc.) is shown in Figure 27.

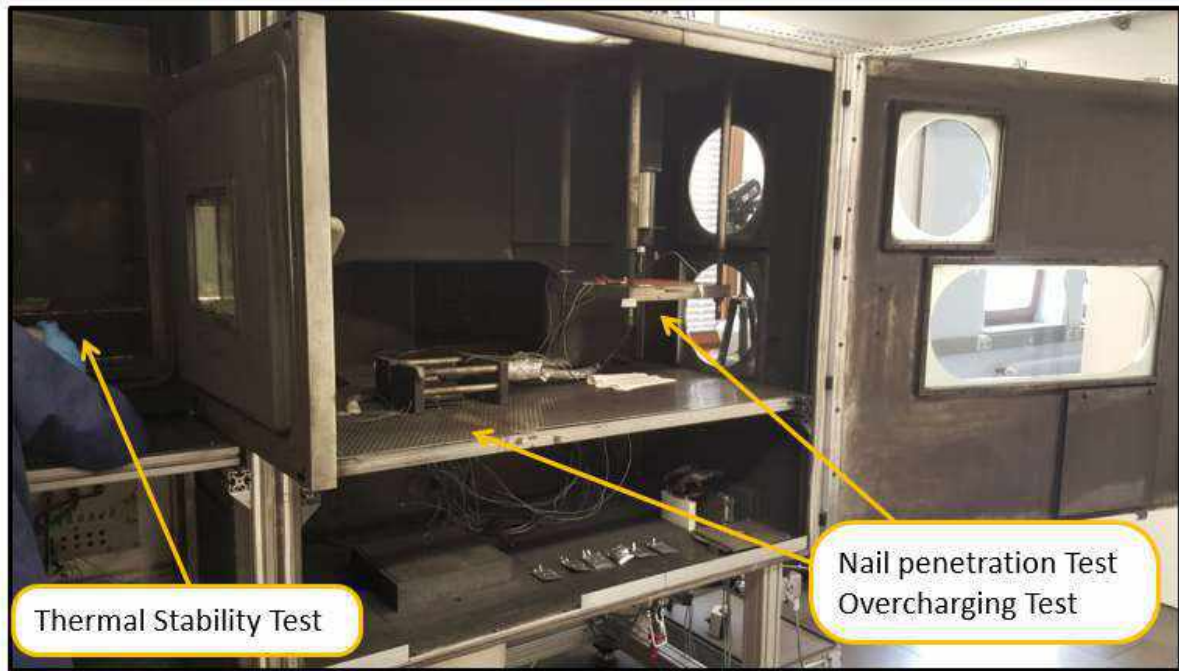


Figure 27: Testing facility.

After the nail penetrates the cell, it's influence on the cell potential and further occurring events are observed.

- Heating Test

The heating tests on the cells were performed by heating the cells up to a temperature of 200 °C. The behaviour of the cells during the heating up and at the end temperature was observed.

- Overcharge test

The test conditions for the overcharge test were the following: A current of 2C (based on 1 Ah cell capacity) was applied to the cell until they reach 24 V, or a safety relevant event occurs.

- Hazard levels

Various hazard levels are defined by EUCAR for the use of a battery in an EV. In Table 1 these hazard levels are listed. It must be noted that in terms of automotive batteries, cells with a hazard level of 4 are often considered as "safe" cells.



Hazard Level	Description	Classification Criteria & Effect
0	No effect	No effect. No loss of functionality.
1	Passive protection activated	No defect; no leakage; no venting, fire, or flame; no rupture; no explosion; no exothermic reaction or thermal runaway. Cell reversibly damaged. Repair of protection device needed.
2	Defect/Damage	No leakage; no venting, fire, or flame; no rupture; no explosion; no exothermic reaction or thermal runaway. Cell irreversibly damaged. Repair needed.
3	Leakage Δ mass < 50%	No venting, fire, or flame*; no rupture; no explosion. Weight loss <50% of electrolyte weight (electrolyte = solvent + salt).
4	Venting Δ mass \geq 50%	No fire or flame*; no rupture; no explosion. Weight loss \geq 50% of electrolyte weight (electrolyte = solvent + salt).
5	Fire or Flame	No rupture; no explosion (<i>i.e.</i> , no flying parts).
6	Rupture	No explosion, but flying parts of the active mass.
7	Explosion	Explosion (<i>i.e.</i> , disintegration of the cell).

Nail Penetration Test automatically leads to HZL:2 (at least)

Table 1: Various hazard levels are defined by EUCAR [7].

4.6.2 Safety Test 1: Nail penetration Test

After the nail penetrated the base line cells and the cell with Level-2 sensor a quite comparable behavior could be detected. The cells with Level-1 sensor could not be tested due to reasons described above (no cell voltage). The penetration of the nail resulted in an immediately drop of the cell voltage. This immediate drop led to an unsuspecting behavior of the cell, as the cell displayed almost no heat generation. While the baseline cell temperature increased by one degree, the Level-2 sensor cells increased by 4 degrees Celsius. This difference is rather attributed to the manual manufacturing process then by the integrated sensor. After the cell potential dropped at puncture, it remains mostly steady or displayed slow decrease over time. Within Figure 28 the resulting safety test data and pictures for the nail penetration test of baseline 1 Ah cells is described. Figure 29 displays the comparable data and picture for tested 1 Ah cells with Level-2 sensor.



Baseline cell (1Ah): cell 11

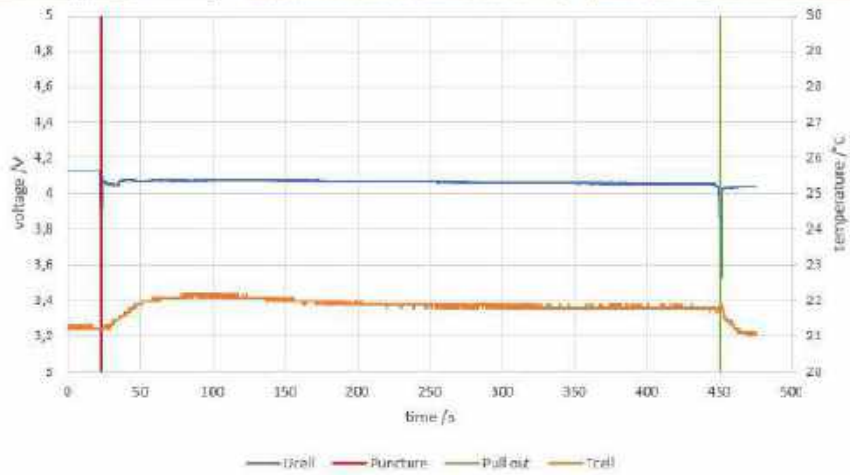
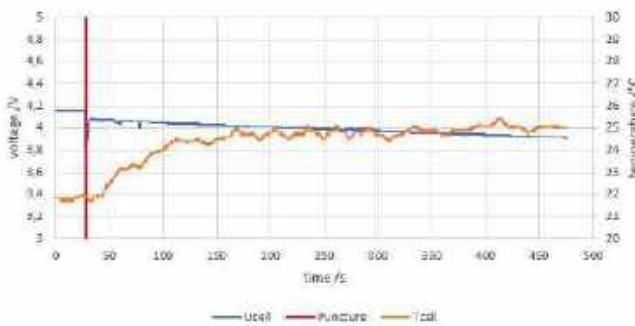


Figure 28: Nail penetration test of 1 Ah baseline cell.

Lvl-2 sensor cell (1Ah): cell 15



Lvl-2 sensor cell (1Ah): cell 16

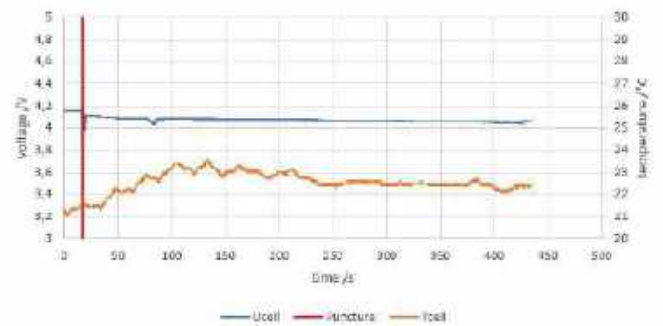


Figure 29: Nail penetration test of 1 Ah cells with integrated Level-2 sensors.



It can be noted that the puncture of the cells with the nail did not result in strong heat generation and possible thermal runaways in the investigated cells. How a thermal runaway would look like is displayed by an example measurement of a different cell in Figure 30 (note: this cell was not used in the project and incorporates different active materials and electrolytes and 0.3 A cell capacity). This type of cell also showed only a slightly cell potential dropped only after being penetrated by the nail but displayed strong heat generation and a thermal runaway within 1-2 minutes afterwards.



Figure 30: Chronological sequence: cell before nail penetrates (left), nail penetrated the cell (middle), thermal runaway (right).

Regarding Hazard levels, the cells used within SENSIBAT would be listed with a Hazard level of 2 up to 4.

4.6.3 Safety Test 2: Heating Test

During the heating safety test the cells were heated up to a temperature of 200 °C, which is displayed in Figure 31, Figure 32, Figure 33 and Figure 34. In blue the cell potential is pictured, while the green and violet line picture the temperature of the oven/environment. The orange lines report the cell temperature respectively.

The cell potential stays quite stable, but after the separator melts it is clearly visible that the cell potential is lost rapidly. The used W-scope separators (see D3.2 [3] for cell specifications) are melting at a temperature of about 165 °C. Figure 31 displays the different cells at the beginning, during and at the end of the heating test. During the test the cells strongly expand with increasing temperature. The reason therefore is that more and more electrolyte components change from liquid to gaseous state. For cells containing Level-1 sensors, almost no volumetric change was observed and further (displayed in Figure 33) also the cell voltage was not comparable. This indicates again the above-described loss of electrolyte due to leakage at the feed-through. The investigated cell with Level-2 Sensor resulted in a thermal event during the heating test. Figure 31 and Figure 34 describe this thermal event occurring at an oven temperature above 160 °C. The baseline cell (displayed in Figure 31 and Figure 32) lost the cell voltage at the temperature at the separator degeneration.



Figure 31: 1 Ah baseline, Level-1, and Level-2 sensor cells during and at the end of the heating test

Baseline cell (1Ah)

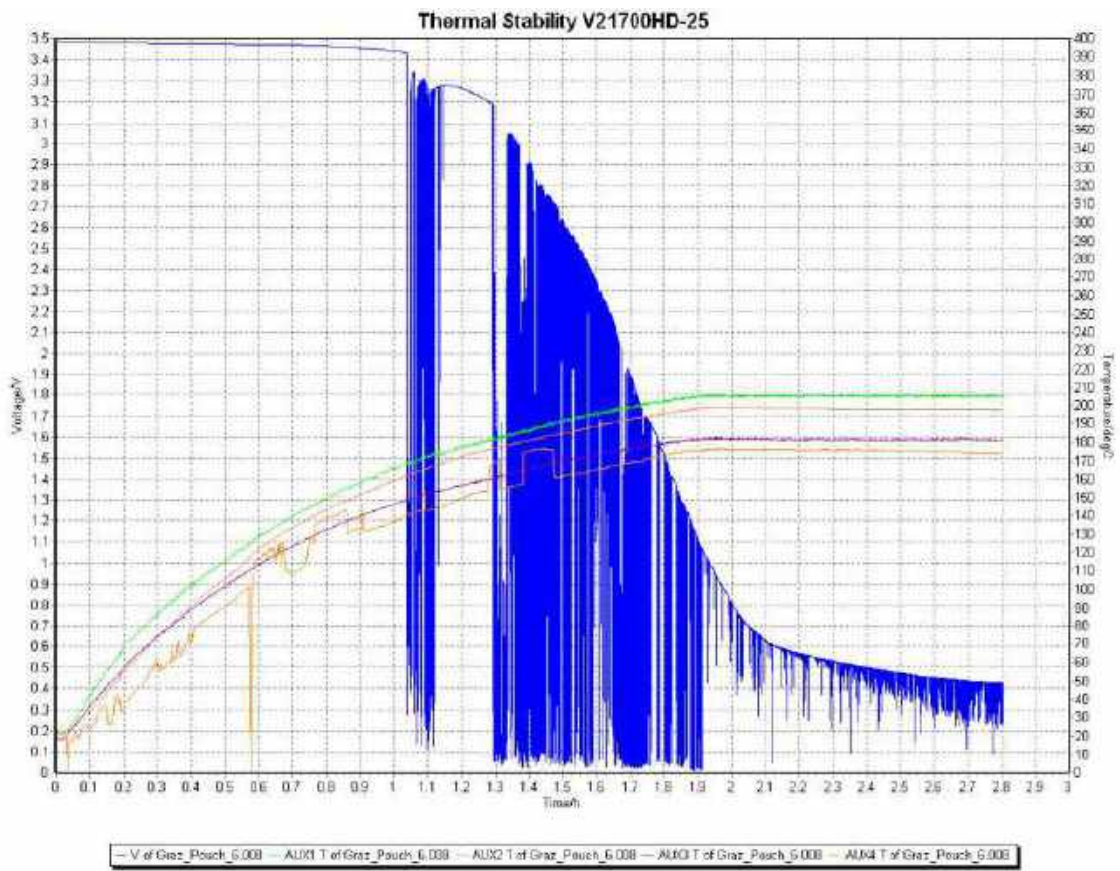


Figure 32: Heating test on baseline cell (1 Ah)



Lvl-1 sensor cell (1Ah)

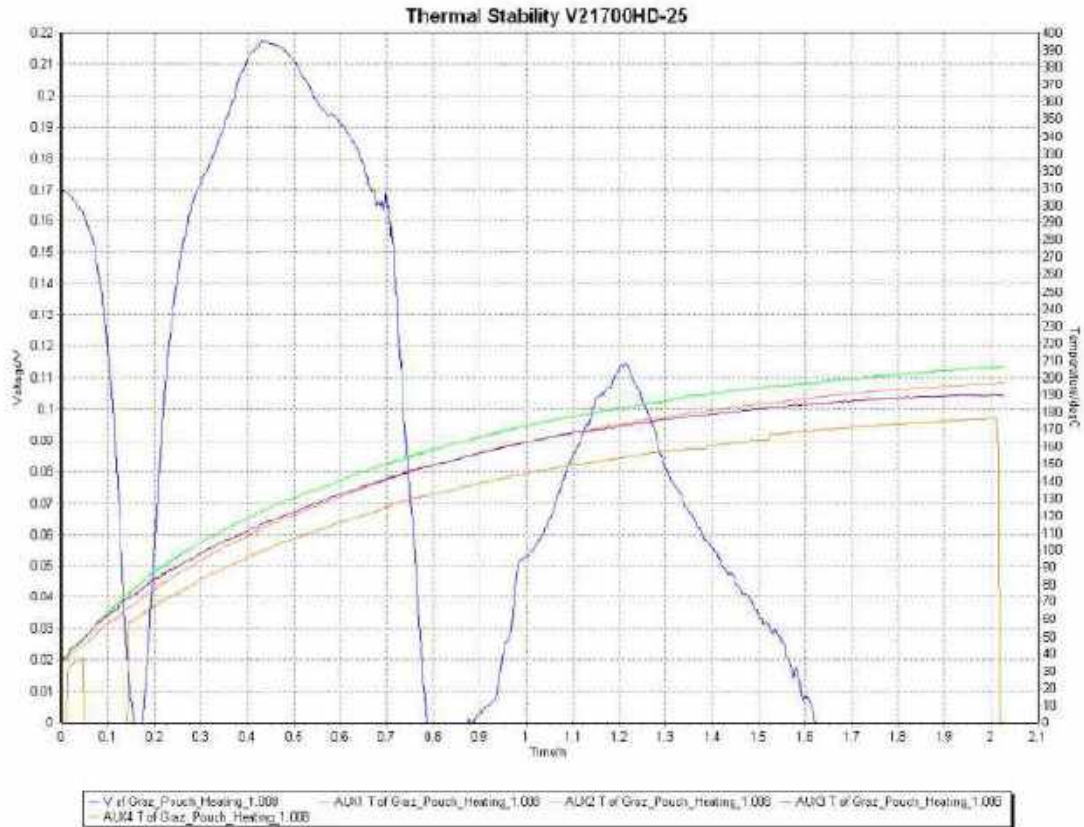


Figure 33: Heating test on cell with Level-1 sensor (1 Ah)

Lvl-2 sensor cell (1Ah)

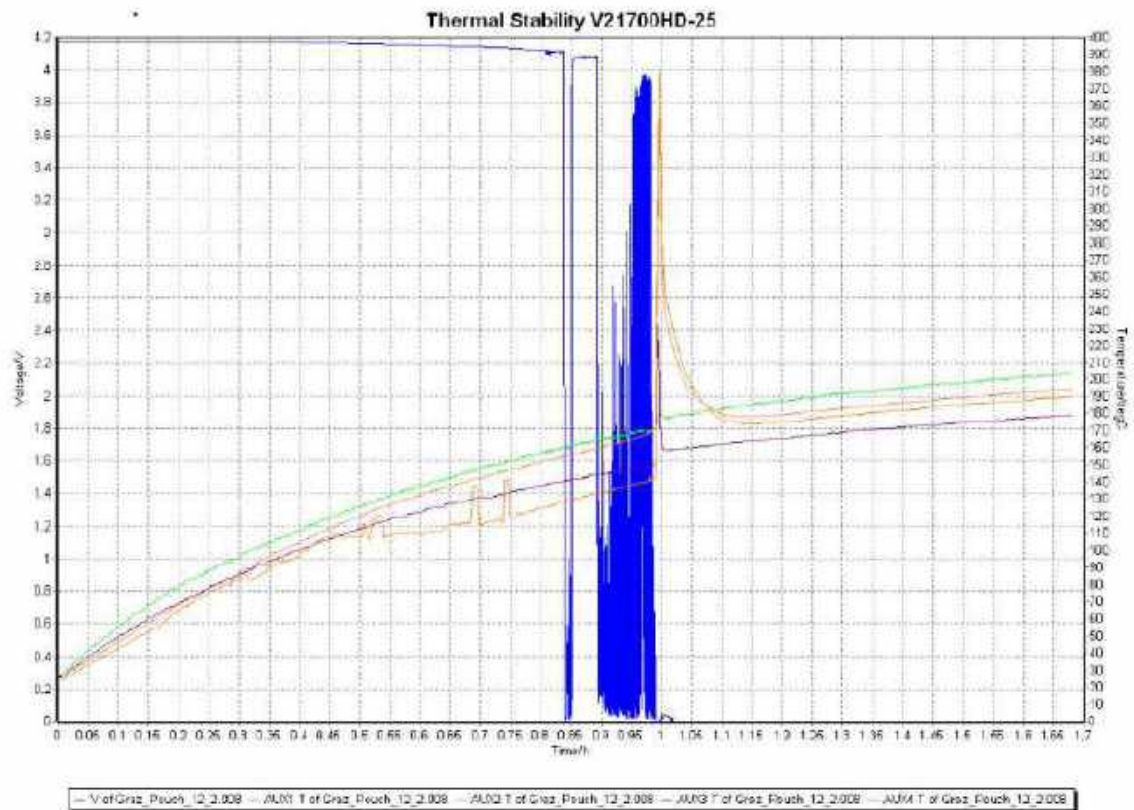


Figure 34: Heating test on cell with Level-2 sensor (1 Ah)



4.6.4 Safety Test 2: Overcharge Test

The third safety test performed was an overcharge test. A current of 2C (based on 1 Ah cell capacity) was applied to the cell until they reached 24 V or a reaction occurred. The safety tests of a baseline cell and two Level-2 cells are displayed in Figure 35 and Figure 36. The blue line indicates the potential of the cell, while the orange line describes the applied current. The grey line gives the temperature, but it must be noted that the measured temperature was often not correctly recorded, due to the reason that the safety-related events were considerable, causing the temperature sensor to be disconnected. For Level-2 cells the yellow line provides information on the potential between the LFP reference and the anode.

While baseline cells reacted very comparable in the test, one of the cells containing a Level-2 sensor allowed operation for almost the doubled duration until a comparable event occurred (almost 40 minutes). This cell may have suffered of self-discharge losing the 30 % storage SOC, which is in-line with the measured, lower cell potential. In general, the Level-2 sensor allowed us to monitor what occurred at the negative electrode. While the cell voltage did not show a significant change the temperature change of the cell is connected to a drop of the anode potential from 3.5 V vs. LFP-reference to 2 V vs. LFP, connected with an unsteady behavior of the potential. This can be associated with dendrite growth occurring on the negative electrode (see Figure 35). Observable in the sample pictures of the connected videos (see Figure 36) is the volumetric change of the cell, which may influence the reference signal as well.

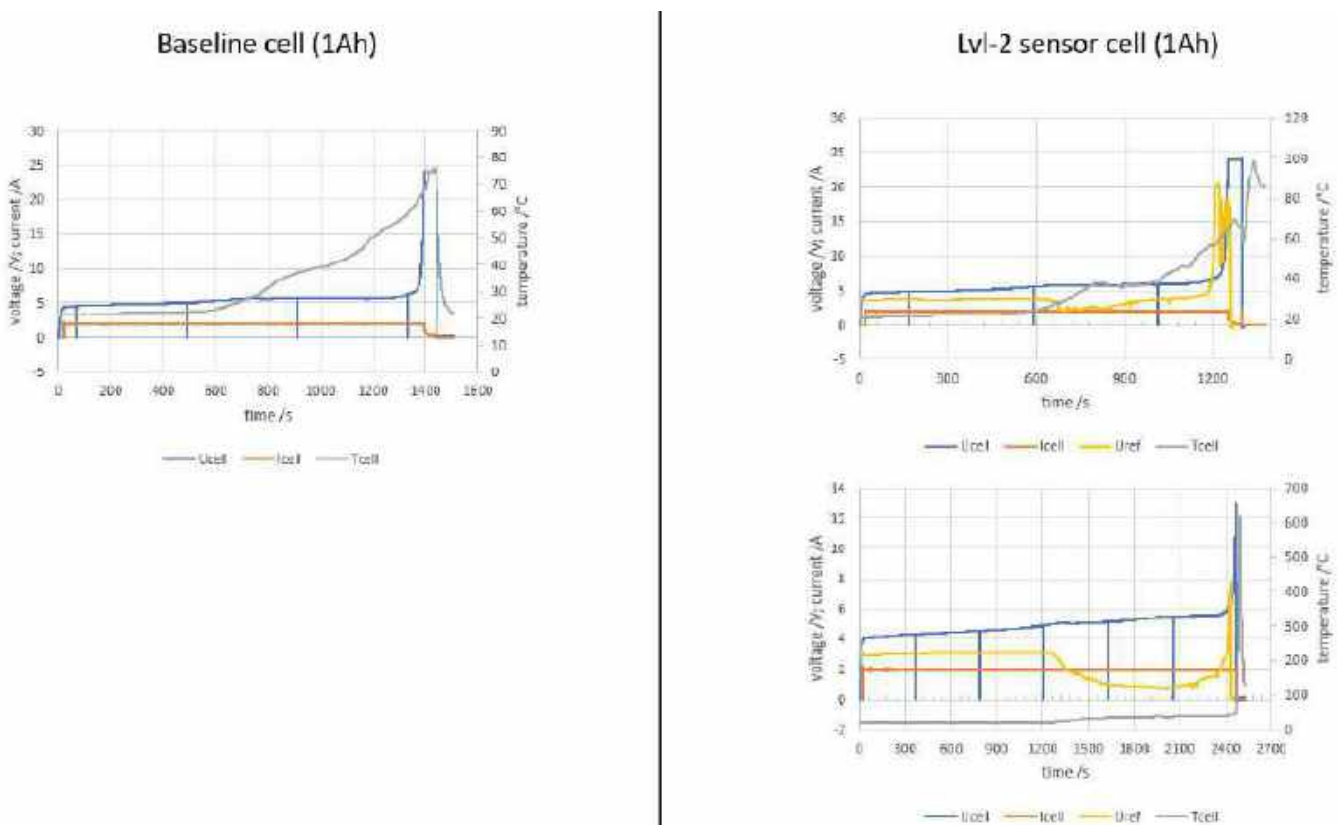


Figure 35: Overcharge test on baseline cell (1 Ah) and cell with Level-2 sensor (1 Ah); Cells with Level-2 sensor provide additional information on the reference voltage (LFP) vs. Anode.

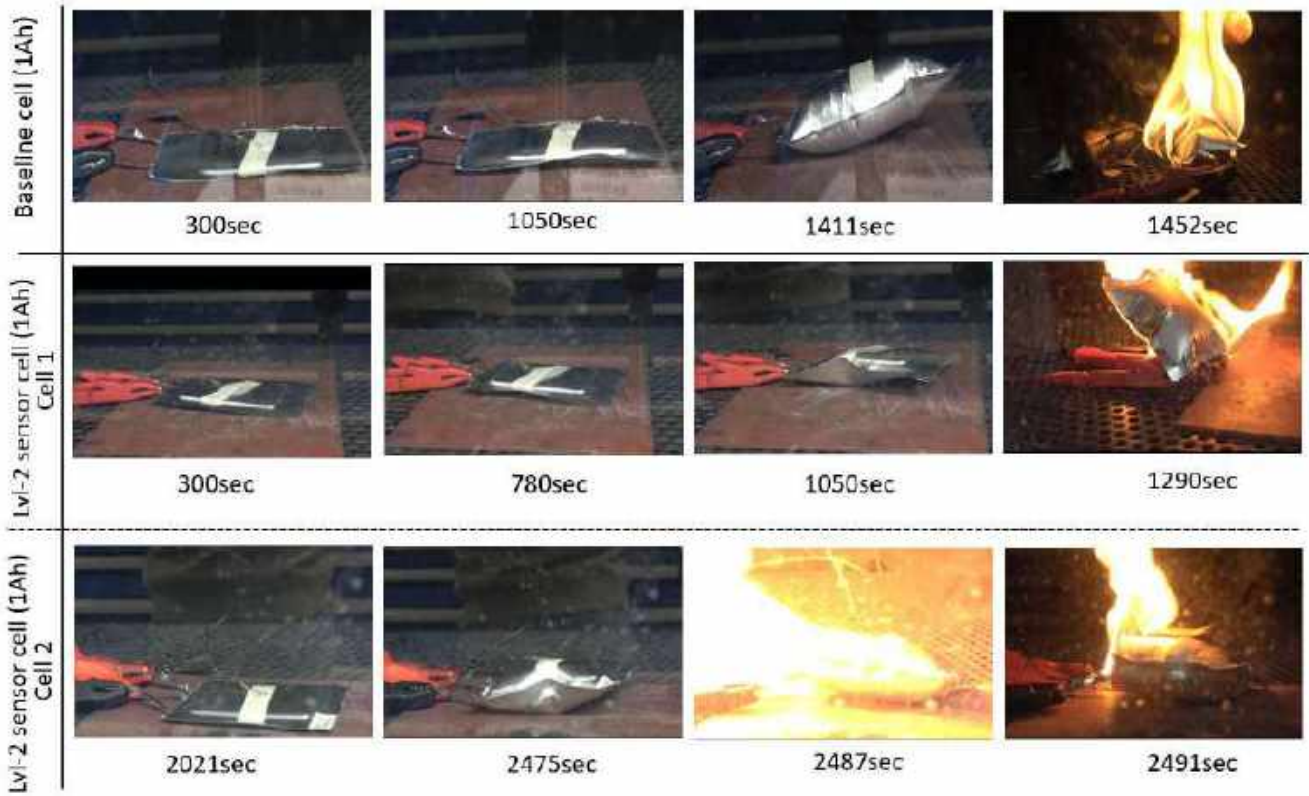


Figure 36: Sample pictures of the videos documenting the Overcharge test on baseline cell (1 Ah) and cell with Level-2 sensor (1 Ah).



5 Algorithm validation

Baseline and improved SOX algorithms exploiting L1 sensors are described in the D4.4 report [5]. First of all, baseline algorithms are developed for both SOC and State of Health (SOH), as well as for State of Safety (SOS). SOH has a value between 0 and 1 and relates the actual maximum capacity at a moment in time to the nominal maximum capacity when the cell was new. SOS is also captured in a value between 0 and 1, where 1 means a perfectly safe cell and a value below 0.8 implies that either all indicators (related to cell voltage, current, temperature rise and correlation between current and voltage sign) are close to their safe limit, which leads to a warning, or one of those indicators is below 0.8, in which case a non-safe state is flagged.

In terms of used data sets, a first data set was used to fit the baseline SOC Equivalent-Circuit Model (ECM). This dataset (dataset 1) is similar to the measurements described in section 4.1 in this D5.1 report. Moreover, a second dataset (dataset 2) was used to validate a baseline SOS algorithm. This second dataset is described in section 4.6 in this D5.1 report. Finally, the dataset described in section 4.2 in this D5.1 report was used as a third dataset. This third aging dataset on baseline cells (dataset 3.1) was used to validate the baseline SOC and SOH algorithms. At the same time, since the L1 sensors could not be properly read out during those experiments as described in section 4.2, the one-dimensional externally measured pressure values obtained from the setup in Figure 9 was used as additional 'L1' sensor data to quantify merits of algorithms exploiting additional sensor data. The dataset where externally measured pressure was available is denoted as dataset 3.2. This led to improved algorithms for SOC, SOH and SOS, and was also used as additional validation for the baseline SOC and SOH algorithms (without exploiting the pressure measurement in that case). Figure 37 summarizes the results for the baseline SOC and SOH algorithm using datasets 3.1 and 3.2.

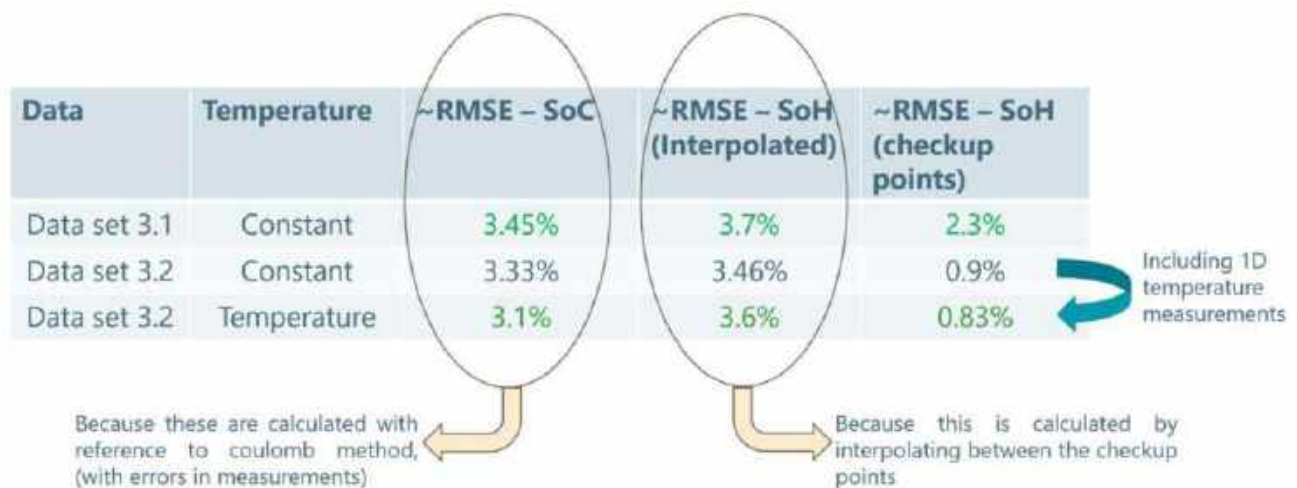


Figure 37: Quantitative results yielded from SOH estimation algorithm for baseline cells.

In the first two lines (dataset 3.1 and first line for dataset 3.2), the temperature was assumed to be constant at 25 °C, even if in the real measurements, this cell temperature was sometimes slightly elevated, particularly when 3C currents were applied in the check-up cycles. The last line shows the situation where the actual measured cell temperature (with an external sensor) is used for the SOC and SOH algorithm. Figure 37 shows that this improves the accuracy of the baseline models. At the same time, for SOH estimation, it was found that the accuracy improves if the estimated and 'real' SOH coming from the check-up measurements are only compared in the check-up points, and not in between where the real SOH is not known and assumed from linear interpolation between the check-up SOH points.



An example of the use of dataset 2 to validate the baseline SOS algorithm is shown in Figure 38.

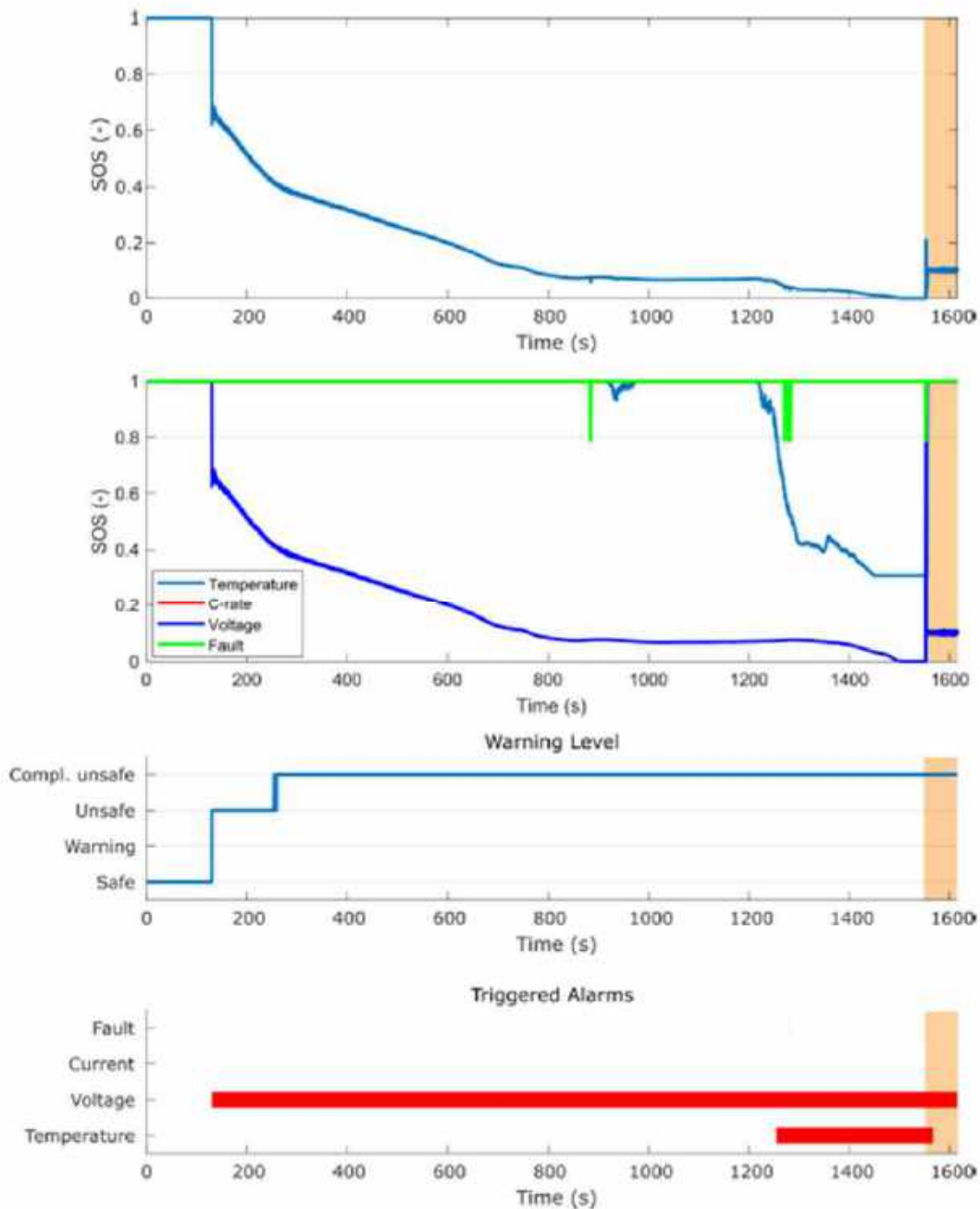


Figure 38: Output of SOS algorithm for overcharge test (Baseline Cell): Overall SOS, SOS by terms, warning level and triggered alarms. Orange shadowed part represents thermal runaway event.

Figure 38 shows the different outputs of the SOS algorithm when executing it with the data from the overcharge test described in section 4.6.4. The first graph shows the overall SOS value, as introduced above. Besides, the second graph shows the decomposition of the overall SOS into its different terms, i.e., each of the safety functions or indicators introduced above: temperature, current, voltage and fault (the latter occurs if the signs of current and voltage do not agree, e.g. the voltage rises for a discharge current). Finally, the last two figures show the warning level (completely unsafe, unsafe, warning and safe operation, according to the defined SOS thresholds) and the triggered alarms (i.e., which SOS term is below 80 %).



For the improved SOH algorithm (from which the SOC algorithm will also benefit since a better SOH algorithm will yield more accurate maximum capacity values over time, which is a crucial parameter in SOC estimation), the pressure measurements using the setup of Figure 9 were exploited in the form of the relation between average pressure at 50 % SOC between charging and discharging pressure (the 'eye') and SOH. An example of such relation obtained from the measurements with the setup of Figure 9 for cell #3 is shown in Figure 39.

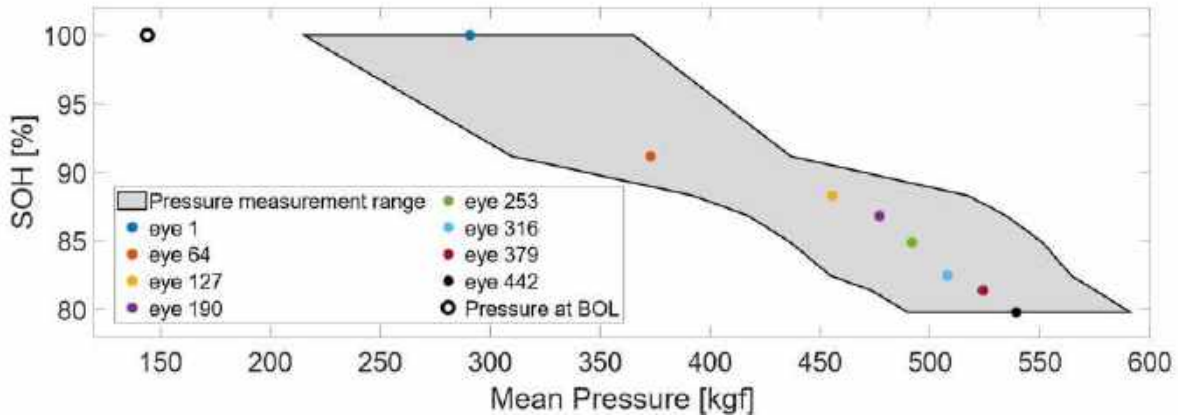


Figure 39: Pressure vs SOH relationship obtained from the measurement data of cell #3 (Dataset 3.2).

The relationship of average pressure ('eye' points recorded at various cycles in the measurements described in section 4.2) and SoH as shown in Figure 39 was used in the form of an equation denoted as Q_{L1} to improve the baseline SoH algorithm (equation explained in deep in the section 4.2 of the D4.4 report [5]). In the baseline SOH algorithm a Weighted-Least-Square (WLS) method was applied to relate differences in SOC over time to actual charge, exploiting the general equation that $\Delta SOC = Q/Q_{max}$, where the ΔSOC comes from the SOC estimator and Q comes from pure Coulomb counting, while Q_{max} is the intended maximum capacity needed for SOH estimation (to relate it to the initial nominal maximum capacity) obtained from a WLS fit between a time series of ΔSOC and Q data points. In the improved method, the Q_{max} obtained from this baseline WLS method was mixed with obtaining it from the Q_{L1} equation coming from the sensor data in Figure 39. Two tuning parameters λ_1 and λ_2 were introduced, where $\lambda_1 + \lambda_2 = 1$, and λ_1 is multiplied with the WLS minimization term in an overall cost function while λ_2 is multiplied with the pressure-function minimization term in the same overall cost function. Therefore, $\lambda_1 = 1, \lambda_2 = 0$ corresponds to the baseline algorithm. The results for cell #3, where the pressure relation Q_{L1} blended in via tuning parameter λ_2 is also obtained for cell #3 (see Figure 39), are shown in Figure 40. The baseline result ($\lambda_1 = 1, \lambda_2 = 0$) corresponds to the grey point and to the value of 0.83 % RMSE, in line with Figure 37. By decreasing λ_1 while increasing λ_2 , keeping the sum equal to 1 for proper blending of baseline WLS to exploiting the pressure sensor data via Q_{L1} , the RMSE value can be significantly decreased. However, this is not completely fair, since cell #3 was validated, and the pressure-versus-SoH curve Q_{L1} exploited in the estimation algorithm was obtained for the same cell. Therefore, the validation was repeated for cell #4. Here, the baseline SOH algorithm yielded an RMSE value of 1.61 %. This is higher than the 0.83% obtained for the baseline algorithm applied to cell #3, due to some consistency issues over time with the measured cell data for cell #4. Still, on inclusion of functional relationship derived from the measurements of cell #3 in Figure 39, and choosing $\lambda_1 = 0.8$ and $\lambda_2 = 0.2$, the RMSE for SOH estimation for cell #4 is 1.53 %. This shows that also in this case, exploiting additional pressure sensor data helps to improve the accuracy of the SOH (and therefore also the SOC algorithm as explained above) algorithm.

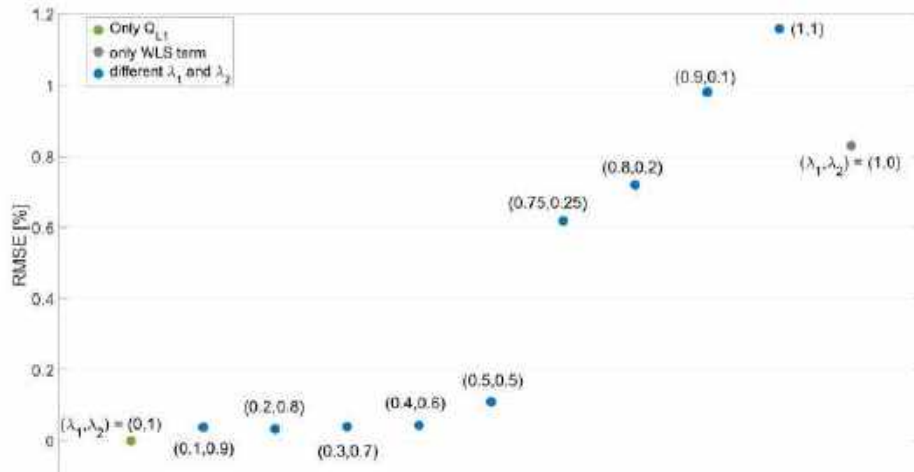


Figure 40: RMSE results with different tuning parameters λ_1 and λ_2 for the cost function J for cell #3 (Dataset 3.2).

Though a safety dataset for the L1 cells was not available (for the cycling data set of section 4.2, no critical situations like thermal runaway were invoked), still the data from dataset 3.2 can be exploited to validate an improved version of the SOS algorithm. In this case, the algorithm was improved by adding indicators related to the relative increase in pressure compared to the Beginning-of-Life (BOL) situation and related to the derivative in pressure. The latter leads to a clear effect on the estimated SOS when the pressure suddenly increases. An example of part of the measurements described in section 4.2, the first Performance Test for cell #4, is illustrated in Figure 41 below. As can be seen, roughly in the middle of the figure, after application of the 3C current in the Performance Test, the pressure suddenly increases and remains higher than before.

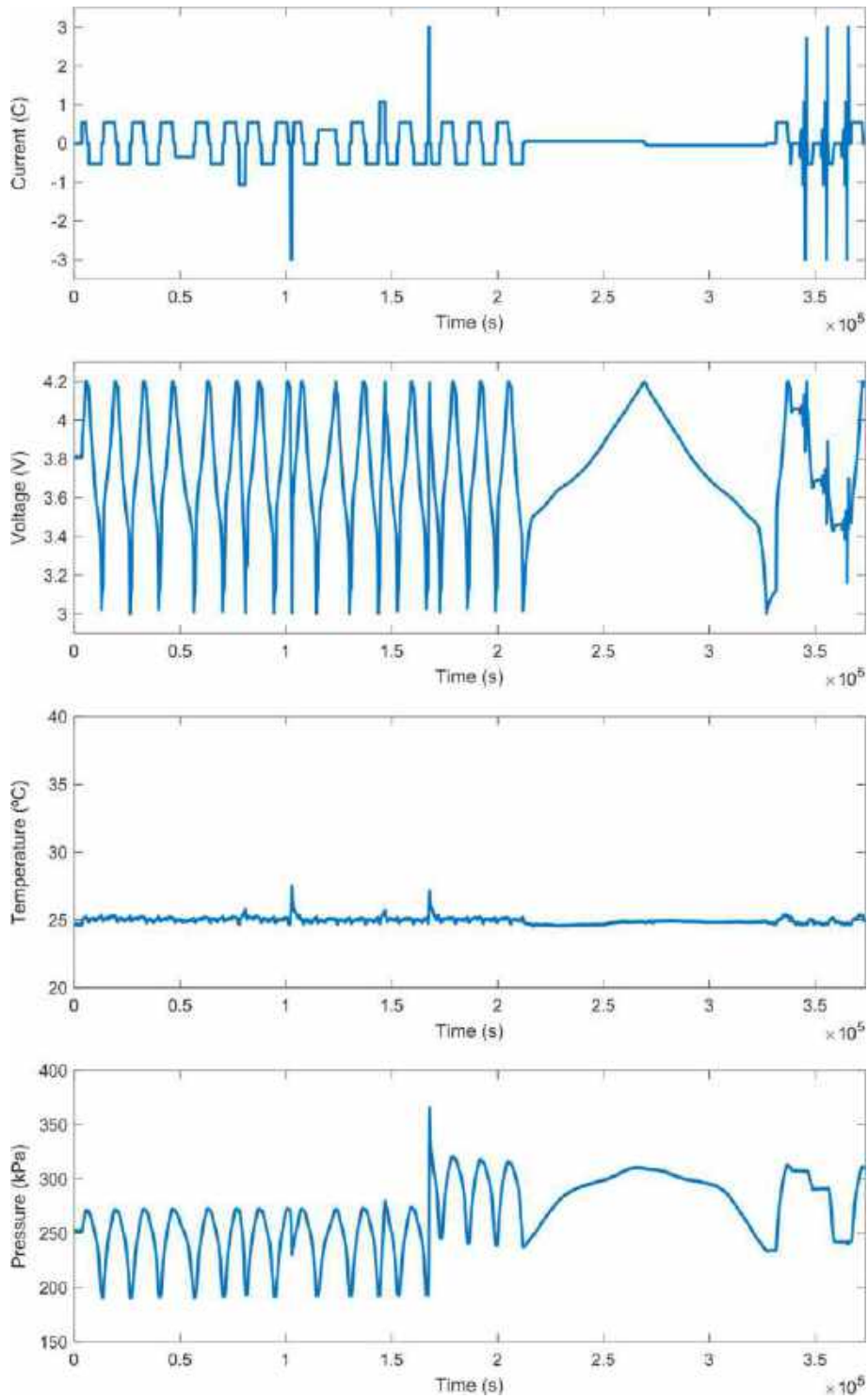


Figure 41: Data recorded in Performance Test #1 (Cell #4, Dataset 3.2): current, voltage, temperature and pressure.

The outputs of the improved SOS algorithm for the measurement results presented in Figure 41 are shown in Figure 42.

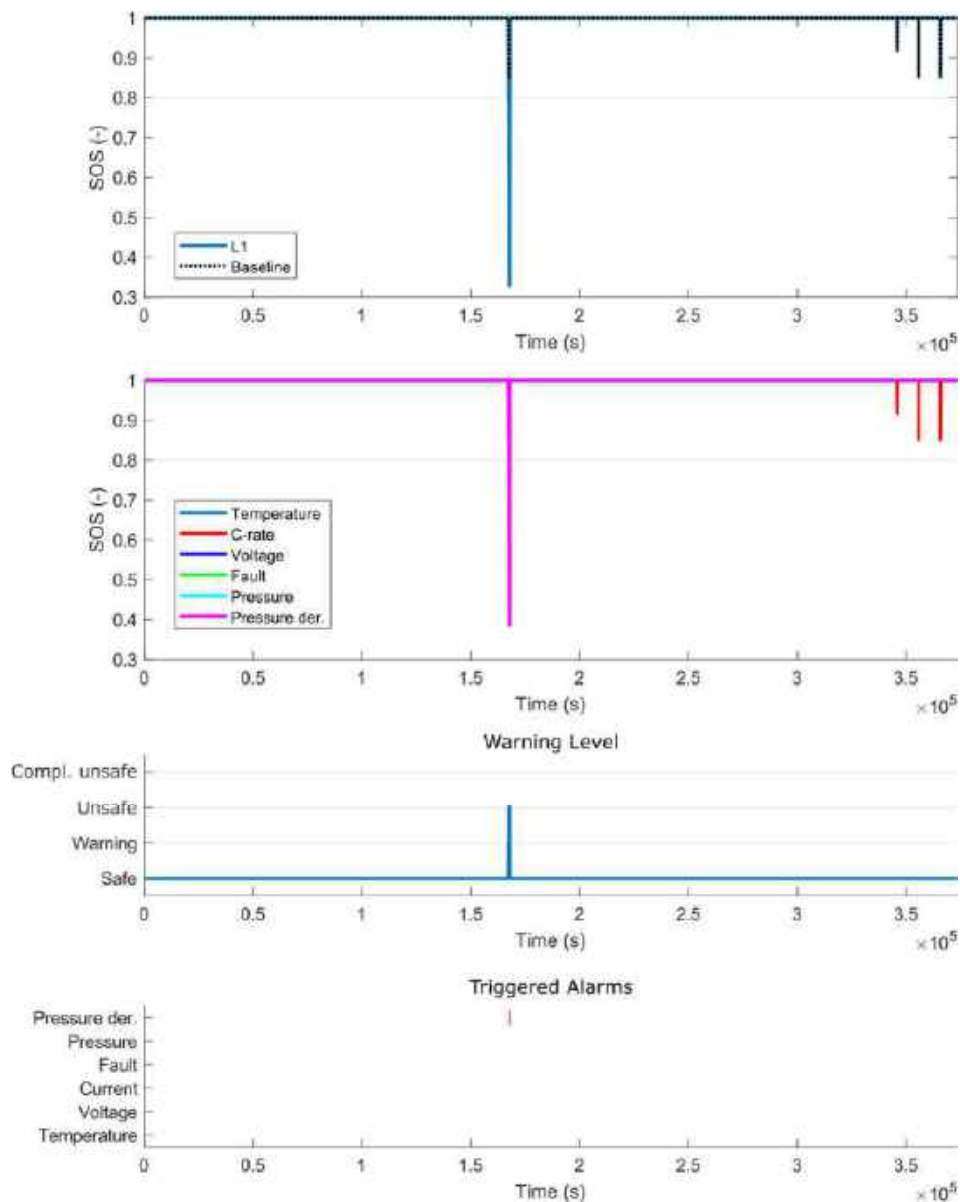


Figure 42: Output of SOS algorithm for Performance Test #1 (Cell #4, Dataset 3.2): Overall SOS, SOS by terms, warning level and triggered alarms.

The results show that there is only one part of the test where an alarm is generated, which coincides with the charging cycle at 3C. During this charge, the pressure increases fast, and the SOS drops until almost the 30 %. During the remainder of the Performance Test, the SOS remains at 100 %, except during the charge pulses at 3C, where the SOS drops a little bit due to the current-related SOS term (C-rate). Further results can be found in D4.5 [6]. In short, the main conclusion is that, due to the addition of the relative pressure and pressure derivative terms, the SOS triggers more alarms as the cell is more aged. Indeed, as the cell ages, its relative pressure increases, what affects the pressure-related SOS term. And eventually, this affects in the overall SOS.

The results of exploiting the individual electrode potentials over time as measured in section 4.4 can be found in the D4.5 report [6]. In fact, the measurement results are exploited to improve the parameter estimation process of a physics-based battery model, in this case the Doyle-Fuller-Newman model. Such a model would be applied in a BMS when more-detailed information about the internal processes and behaviours inside the cell is needed to derive internal states, for example to control charging while minimizing the effect of aging. For something like this to work, it is important that while the model accurately models the cell output voltage (which



can be compared to a measured cell voltage in an observer to estimate internal states), the internal states are accurately described. For this to happen, it is important that the parameters, of which there are many in the DFN model, are accurate and have a physical meaning.

The D4.5 report describes how to obtain individual anode and cathode potentials (versus an ideal 0 V reference instead of the actually applied 3.41 V LFP reference electrode or L2 sensor) from the measurements described in section 4.4. For example, the individual cathode and anode potentials are shown together with the cell voltage ($V_{\text{cell}}=V_{\text{cathode}}-V_{\text{anode}}$) in Figure 43 for the pulse discharge test of Figure 14.

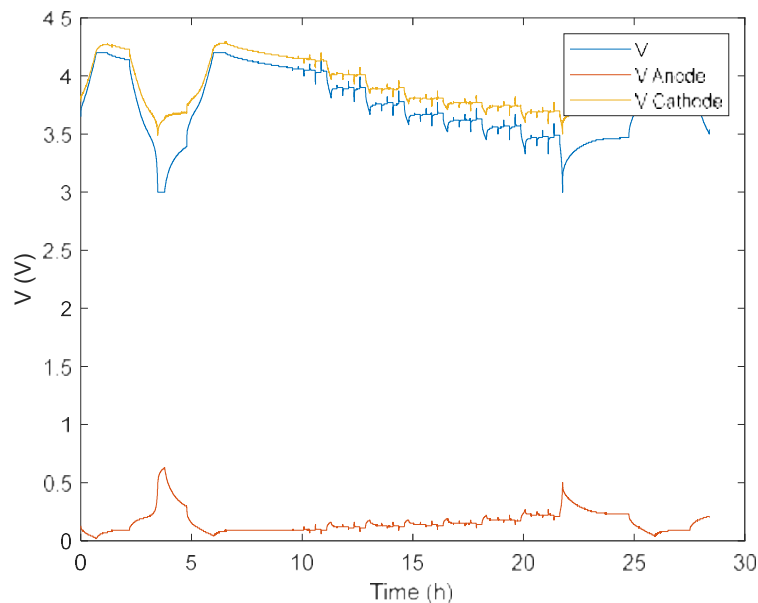


Figure 43: Calculated voltage responses of the anode (red curve) and cathode (yellow curve) (both versus an ideal 0V reference), as well as the measured cell voltage (blue curve) for the Hybrid Pulse Discharge test.

The curves from Figure 43 were used to derive the OCV curves of the individual electrodes, which were then used in the DFN model in the improved parameter estimation routine. In the original parameter estimation routine, the OCV curve of the anode was assumed from literature, where the OCV curve of the cathode was obtained by adding this assumed anode OCV curve to the OCV curve derived from the cell voltage from a discharge pulse test. Therefore, the modified method is expected to use better fits for the individual electrode voltages without sacrificing the accuracy of the overall cell voltage. With the OCV curves in the DFN model being defined either assuming a curve from literature (original procedure) or using the actually measured ones (improved procedure), the drive cycle results from section 4.4 are used to derive the actual model parameters. The results of the original parameter estimation routine are shown in Figure 44, while the results of the improved parameter estimation routine exploiting the reference L2 measurements are shown in Figure 45.

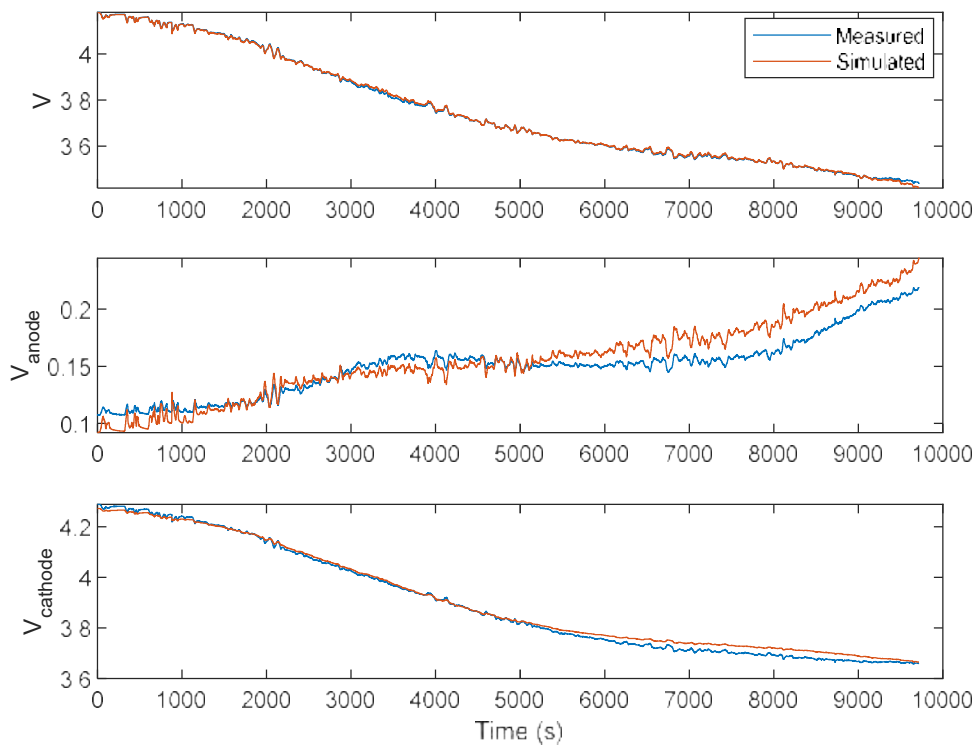


Figure 44: Comparison of measured and simulated voltage responses of the overall cell and respective electrodes (versus an ideal 0V reference) with the original parameter estimation procedure. The measured anode and cathode voltage curves (blue) were NOT used in the parameter estimation routine.

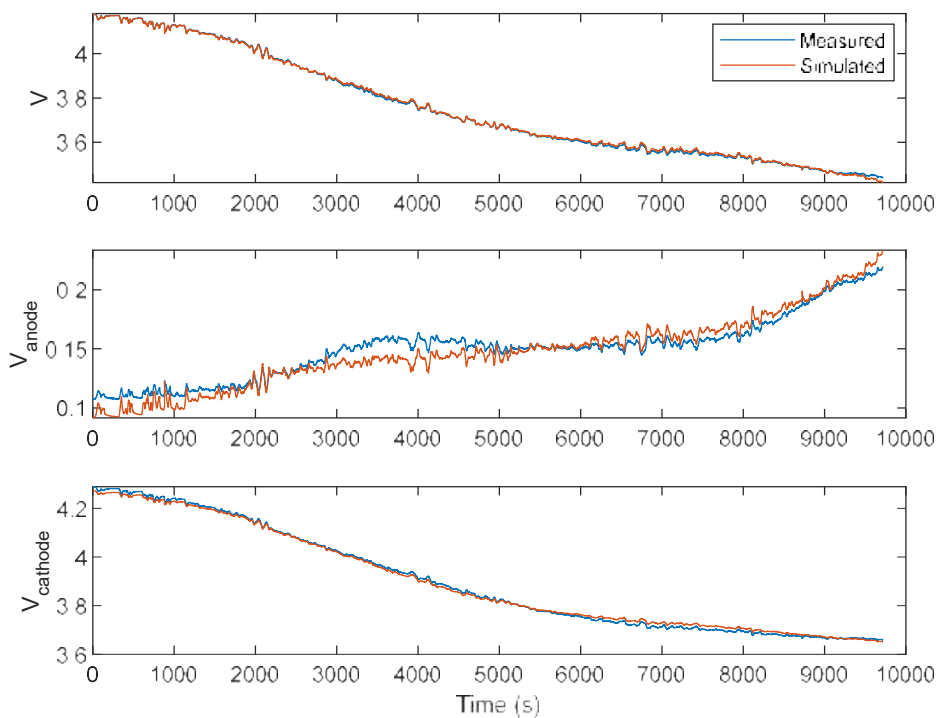


Figure 45: Comparison of measured and simulated voltage Response of the overall cell voltage and respective electrodes (versus an ideal 0V reference) with an adjusted parameter estimation procedure. The measured anode and cathode voltage curves (blue) were used in the parameter estimation routine.



Comparing Figure 45 to Figure 44, it can already visually seen that the electrode voltages better fit the measured ones for the improved parameter estimation routine exploiting the reference electrode measurements in Figure 45, while not visually affecting the accuracy of the overall modelled cell voltage. This is confirmed quantitatively in Table 2 below.

Voltage RMSE values [mV]	Cell Voltage	Anode voltage (versus ideal 0V reference)	Cathode voltage (versus ideal 0V reference)
Original Procedure (corresponds to results in Figure 44)	4,52	13,64	16,45
Modified procedure exploiting measured OCV curves as well as drive cycles (corresponds to results in Figure 45)	5,49	8,71	9,88

Table 2: Comparison of accuracies (Root-Mean-Square Errors (RMSE)) of measured data vs modelled output for the original and improved parameter estimation routines.

Finally, the D4.5 [6] deliverable report also describes how better fitted physical models as the one corresponding to Figure 45 can be exploited to obtain better algorithms. For example, when applying a physics-based model, as described above, the sole reason of doing so is to link an externally measurable variable like cell voltage to internal behaviour. With an improved parameter estimation process, as discussed above, electrode potentials are more accurately modelled, so this also means that overpotentials will be more accurately modelled. As a result, any SOX algorithm relying on an accurate description by the model of what is going on inside the battery will benefit. Particularly, the accuracy of the SOH algorithm based on a physics-based model including aging will improve, simply because the aging model will more accurately describe how capacity is lost and film resistances are increasing. Moreover, e.g., terms can be added to the overall SOS equation as is done in in the D4.4 report [5] when adding L1 sensor data. When one modelled equation starts to run faster than a certain defined threshold, the corresponding factor in the overall SoS equation can be decreased further, leading to a lower SOS value.



6 Module and Component Validation

The design of the battery module must be such that it allows for the verification of the internal sensors, as well as the models and strategies developed in the project. A thorough overview of the design of this module can be found in battery module design documentation (D4.3 - BMS-slave—equipped battery module based on the series connection of at least six 5ah prototype pouch cells with level 1 sensors [4]).

The module serves as a test platform to mount all the components developed in this project. It also has an array of sensors that can provide valuable insights and validation. Underneath an image of the almost finalised module. The module has been designed so that the components are well visible, for demonstration purposes, in a safe and attractive package.

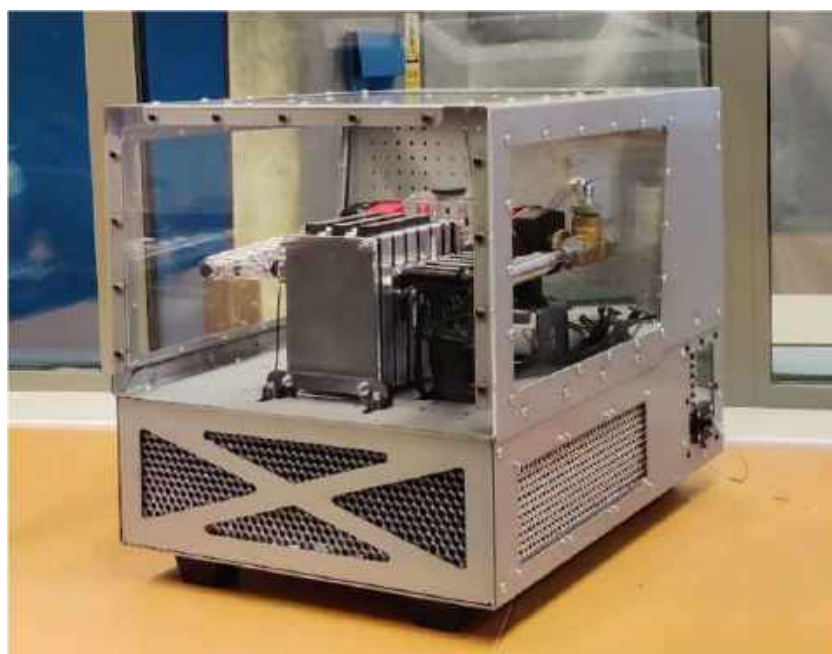


Figure 46: Module overview.

This module contains six cells that are cooled using custom made cooling blocks as discussed in the battery module design document (deliverable D4.3 [5]). Each cell has a thermocouple placed in the centre to be used as validation for the cell temperature. Three load cells are used to measure the total pressure in the cell stack. By comparing the forces of these three sensors it can be ensured that the cell stack is clamped uniformly. The inlet/outlet temperature and flow rate of each of the cooling blocks are measured for validation of the thermal model. All sensors are read out using a Beckhoff PLC. The load cells were calibrated using a lab scale, the flow rate sensors have a calibration document from the supplier and the thermal sensors will be calibrated inside a climate chamber along with the channel readout PCB's.

The module can be placed on an electrical cabinet in which the Beckhoff PLC along with the power supplies can be mounted. The module can also be taken off the electrical cabinet and, for example, placed inside a climate chamber for calibration or testing.

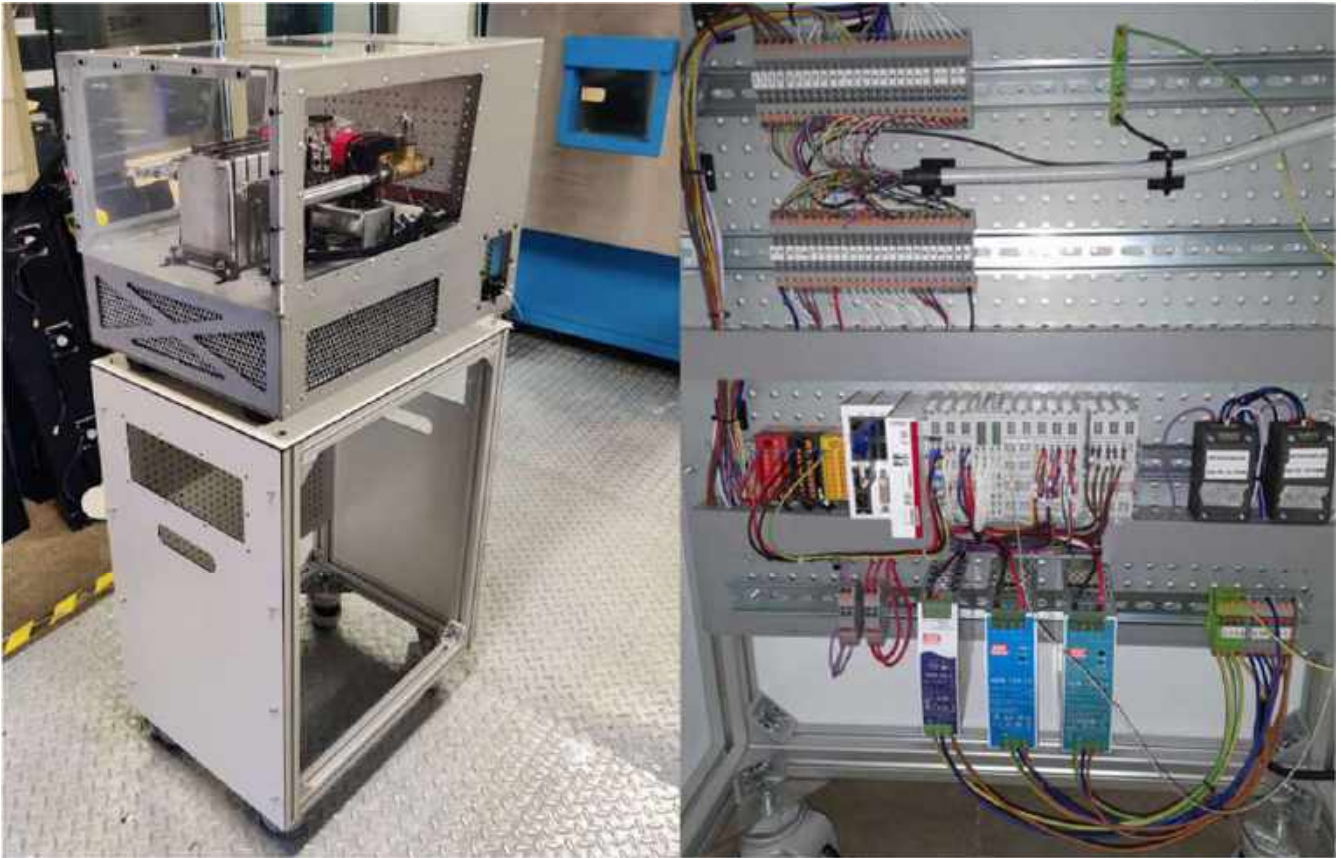


Figure 47: Module and electrical cabinet.

On the back of the module there is room for mounting the PMDU, BMS master and BMS slave. This will be finalised when these components are ready.

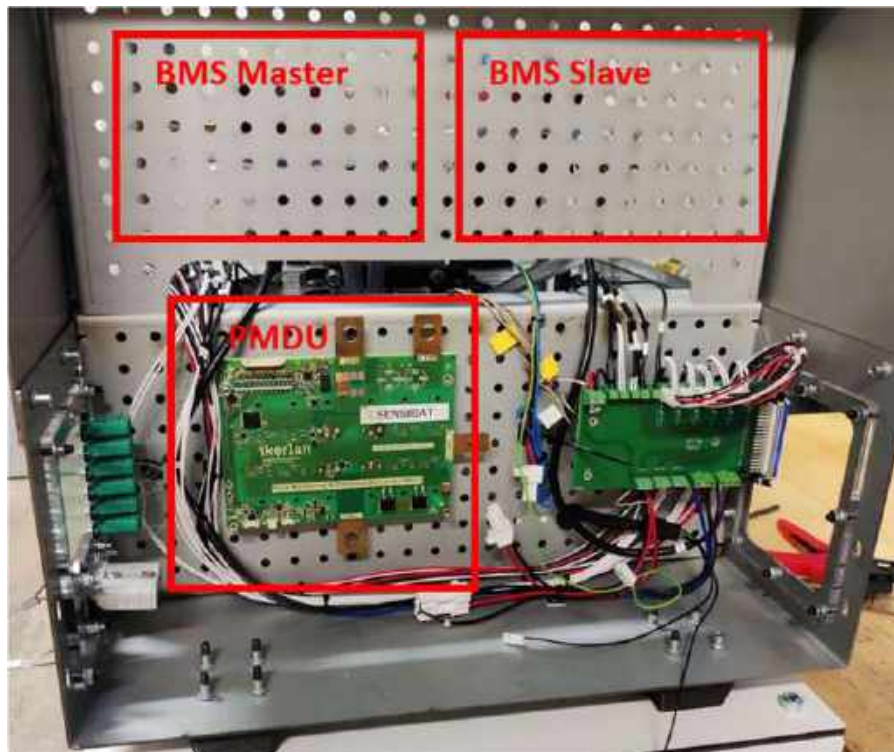


Figure 48: PMDU - BMS master - BMS slave.



6.1 Functional Safety Analysis

Based on a generic analysis the safety objectives for the battery module, the safety related functions of the BMS-Slave can be derived, and a safety integrity level capability is assigned. The results are summarized below.

ID	Safety Objectives	ID	Safety Related Functions	ASIL capability
O1.1	Avoid over-charging and overvoltage	S1	Measurement and monitoring of the voltage across every battery cell	ASIL D
O1.2	Avoid over-discharge and undervoltage			
O1.3	Avoid recharge after undervoltage event			
O2.1	Avoid overtemperature	S2	Measurement and monitoring of the temperature of every battery cell	ASIL D
O2.3	Avoid under-temperature in operating conditions			
O3.1	Avoid overcurrent in charging direction	S3	Measurement and monitoring of the current of the battery module	ASIL D
O3.2	To avoid overcurrent in discharging direction			

Table 3:Functional safety analysis table.

Any safety related function consists of 3 generalized parts – sensor, processing, actuator. Here, the BMS-Slave covers the sensor part of the safety related function. Using the AFE developed by Partner NXP it is possible to reach the assigned ASIL capability for the complete safety related function.

The input from the Level-1 sensor matrixes can add another layer information that can be used for plausibility checking and temperature sensor verification. The underlying homogeneity information on temperature and pressure distribution over the cell surface can serve as an early warning to detect anomalies before an actual fault becomes apparent.

Uneven temperature and pressure distribution on the cell surface can indicate uneven current distribution, leading to accelerated local cell degradation. Localized hot spots and pressure spikes can indicate onsetting Lithium plating. Subsequently, this may lead to dendrite growth and local puncture of the separator.

In combination with an ASIL D capable AFE the Level-1 sensors can contribute to increase system reliability and safety. A perspective integration of the Level-1 read-out electronics as part of the AFE will help to leverage these advantages.



7 Discussion & Conclusion

Various tests (Performance Test, EIS, Cycle-Life test, Calendar-Life test, Pulse-Discharge test, Drive-cycle test) have shown that the integration of the in SENSIBAT developed L1 and L2 sensor units do only slightly influence main performance indicators like complex resistance, discharge capacity at certain C-rates, and ohmic pulse discharge resistances of the cells.

Furthermore, the L1 sensor demonstrated no discernible impact on the cycle ageing of the SENSIBAT cells. These findings suggest a parity in performance between the L1 and baseline cells, implying that the introduction of the L1 sensor did not adversely affect the cycle-ageing characteristics of the SENSIBAT cells under the given testing conditions. This alignment in performance underscores the potential compatibility and effectiveness of the L1 sensor, providing valuable insights into the overall robustness and resilience of the cells in the presence of this sensor technology.

Regarding the storage capability of the cells with integrated L1 sensors, based on post-mortem analysis it must be concluded that the L1 sensor integration has a long-term influence on the integrity of individual cell components. It can be assumed that the used material combination for the L1 sensor encapsulation (Parylene C) and the melting layer of the pouch foil (PP) does not produce a satisfactory sealing. Further investigations must be conducted in order to tackle this issue and find a suitable solution for not leaking pouch cells.

The safety tests also showed no abnormalities in the L1 and L2 cells compared to the baseline cells. In summary, it can be stated that the integration of the developed sensors has no influence on the safety of the cells.

While individual components of the module underwent meticulous manufacturing and validation processes, a critical limitation arose during the course of the SENSIBAT project. Regrettably, the validation test of the L1-5Ah cells-based module faced an impediment due to the unavailability of essential working electronics, including readout electronics, BMS slave, and BMS master, before the project's conclusion. This unforeseen challenge resulted in the inability to conduct a real-module-level validation of the cells and algorithms that had undergone rigorous validation at the cell level as depicted in the present document. Despite the extensive efforts invested in ensuring the thorough evaluation of individual components, this unforeseen constraint highlights the complexity and interconnected nature of the validation process, underscoring the need for a comprehensive and synchronized approach in future endeavours within the realm of battery technology research and development.



8 References

- [1] D1.1 Requirement Specification (Use cases, KPIs and cell, module requirements, SENSIBAT, January 2021)
- [2] D1.2 Testing plan for cells and modules, SENSIBAT, March 2021
- [3] D3.2 Report on prototyping baseline pouch battery cells, SENSIBAT, April 2021
- [4] D4.3 BMS-slave—equipped battery module based on the series connection of at least six 5ah prototype pouch cells with level 1 sensors, June 2023
- [5] D4.4 Advanced module-level state estimators based on level 1 sensors, December 2023
- [6] D4.5 Advanced state estimation algorithms based on level 2 sensors, December 2023
- [7] EUCAR Hazard Levels Classification and Description



9 Acknowledgement

The author(s) would like to thank the partners in the project for their valuable comments on previous drafts and for performing the review.

Project partners

#	PARTICIPANT SHORT NAME	PARTNER ORGANISATION NAME	COUNTRY
1	IKE	IKERLAN S. COOP.	Spain
2	BDM	BEDIMENSIONAL SPA	Italy
3	POL	POLITECNICO DI TORINO	Italy
4	FHG	FRAUNHOFER GESELLSCHAFT ZUR FOERDERUNG DER ANGEWANDTEN FORSCHUNG E.V.	Germany
5	FM	FLANDERS MAKE VZW	Belgium
6	TUE	TECHNISCHE UNIVERSITEIT EINDHOVEN	The Netherlands
7	NXP NL	NXP SEMICONDUCTORS NETHERLANDS BV	The Netherlands
8	NXP FR	NXP SEMICONDUCTORS FRANCE SAS	France
9	ABEE	AVESTA BATTERY & ENERGY ENGINEERING	Belgium
10	VAR	VARTA MICRO INNOVATION GMBH	Germany
11	AIT	AIT AUSTRIAN INSTITUTE OF TECHNOLOGY GMBH	Austria
12	UNR	UNIRESEARCH BV	The Netherlands

DISCLAIMER/ ACKNOWLEDGMENT



Copyright ©, all rights reserved. This document or any part thereof may not be made public or disclosed, copied, or otherwise reproduced or used in any form or by any means, without prior permission in writing from the SENSIBAT Consortium. Neither the SENSIBAT Consortium nor any of its members, their officers, employees or agents shall be liable or responsible, in negligence or otherwise, for any loss, damage or expense whatever sustained by any person as a result of the use, in any manner or form, of any knowledge, information or data contained in this document, or due to any inaccuracy, omission or error therein contained.

All Intellectual Property Rights, know-how and information provided by and/or arising from this document, such as designs, documentation, as well as preparatory material in that regard, is and shall remain the exclusive property of the SENSIBAT Consortium and any of its members or its licensors. Nothing contained in this document shall give, or shall be construed as giving, any right, title, ownership, interest, license, or any other right in or to any IP, know-how and information.

This project has received funding from the European Union's Horizon 2020 research and innovation programme under grant agreement No 957273. The information and views set out in this publication does not necessarily reflect the official opinion of the European Commission. Neither the European Union institutions and bodies nor any person acting on their behalf, may be held responsible for the use which may be made of the information contained therein.